iScience

CellPress
OPEN ACCESS

Article

CD95/Fas protects triple negative breast cancer from anti-tumor activity of NK cells

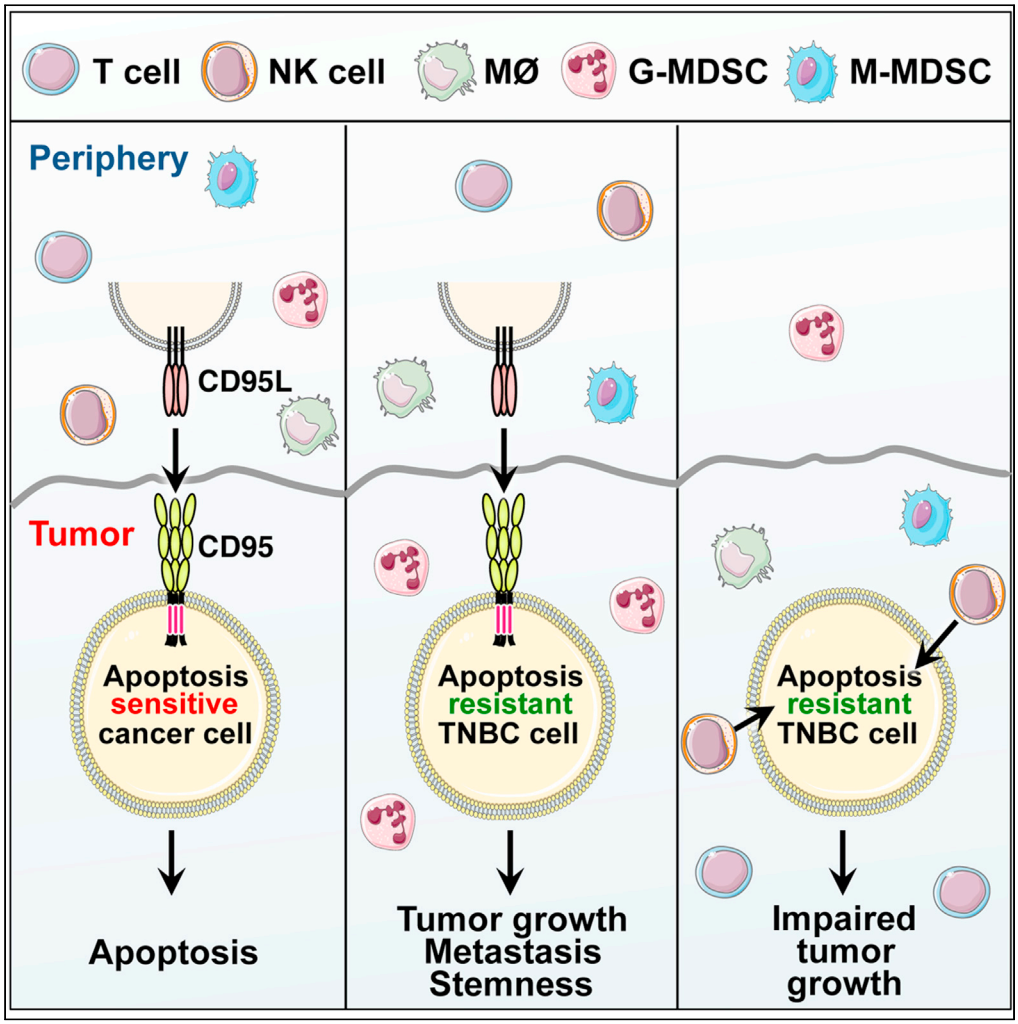

Abdul S. Qadir, Jean Philippe Guégan, Christophe Ginestier, ..., Zhe Ji, Patrick Legembre, Marcus E. Peter

m-peter@northwestern.edu (M.E.P.)
patrick.legembre@inserm.fr (P.L.)

Highlights

CD95 expression promotes primary TNBC growth in immune-competent mice

CD95 KO TNBC cells do not metastasize in immune-deficient mice

Loss of CD95 triggers a pro-inflammatory program affecting the immune landscape

Loss of CD95 causes tumor destruction by NK cells in immune-competent mice

Qadir et al., iScience 24, 103348
November 19, 2021
https://doi.org/10.1016/j.isci.2021.103348

iScience

CellPress
OPEN ACCESS

Article

CD95/Fas protects triple negative breast cancer from anti-tumor activity of NK cells

Abdul S. Qadir,[1,10,12] Jean Philippe Guégan,[2,10] Christophe Ginestier,[3] Assia Chaibi,[2] Alban Bessede,[2] Emmanuelle Charafe-Jauffret,[3] Manon Macario,[3] Vincent Lavoué,[4] Thibault de la Motte Rouge,[5] Calvin Law,[1] Jacob Vilker,[1] Hongbin Wang,[6] Emily Stroup,[6] Matthew J. Schipma,[7] Bryan Bridgeman,[1] Andrea E. Murmann,[1] Zhe Ji,[6,8] Patrick Legembre,[9,11,*] and Marcus E. Peter[1,7,11,13,*]

SUMMARY

The apoptosis inducing receptor CD95/Fas has multiple tumorigenic activities. In different genetically engineered mouse models tumor-expressed CD95 was shown to be critical for cell growth. Using a combination of immune-deficient and immune-competent mouse models, we now establish that loss of CD95 in metastatic triple negative breast cancer (TNBC) cells prevents tumor growth by modulating the immune landscape. CD95-deficient, but not wild-type, tumors barely grow in an immune-competent environment and show an increase in immune infiltrates into the tumor. This growth reduction is caused by infiltrating NK cells and does not involve T cells or macrophages. In contrast, in immune compromised mice CD95 k.o. cells are not growth inhibited, but they fail to form metastases. In summary, we demonstrate that in addition to its tumor and metastasis promoting activities, CD95 expression by tumor cells can exert immune suppressive activities on NK cells, providing a new target for immune therapy.

INTRODUCTION

CD95/Fas is a well-characterized death receptor that in permissive cells or when cross-linked in cancer cells *in vitro* mediates induction of apoptosis when stimulated by its cognate ligand CD95L (Krammer, 2000; Nagata, 1999; Peter et al., 2003). It is now well established that CD95 also has multiple nonapoptotic functions (Guegan et al., 2020; Peter et al., 2007; Wajant et al., 2003). Many of these activities are tumor promoting (reviewed in Martin-Villalba et al., 2013 and Peter et al., 2015) and different mechanisms have been identified that regulate whether CD95 mediates apoptosis or survival (Algeciras-Schimnich et al., 2002; Feig et al., 2007; Gulculer Balta et al., 2019). We previously demonstrated that neither a low-grade serous nor an endometrial ovarian cancer, nor a chemically (diethylnitrosamine, DEN) induced liver cancer, efficiently grew in mice after tissue-specific deletion of CD95 in the ovaries or the liver, respectively (Chen et al., 2010; Hadji et al., 2014). In fact, in all three models either no tumors formed or their numbers and sizes were severely reduced. Interestingly, all tested DEN-induced liver cancer nodules or low-grade ovarian cancer that formed in mice still expressed CD95 (Hadji et al., 2014), indicating that these tumors were escapers caused by the inefficiency of Cre recombination used to delete CD95 and pointing at a pivotal role of CD95 in cancer cell survival *in vivo*. However, it was not clear whether this activity of CD95 was cell autonomous or required cells of the tumor microenvironment.

Among women, breast cancer (BC) is the most common cause of cancer and the second leading cause of cancer death (DeSantis et al., 2016). BC is a heterogeneous disease whose molecular classification distinguished luminal A and B expressing hormonal receptors, basal/triple negative breast cancer (TNBC), and human epidermal growth factor receptor 2 (HER2)-like tumors. This molecular taxonomy is clinically relevant with basal/TNBC patients presenting the poorest clinical outcome with no targeted therapies available compared with other molecular subtypes. TNBCs progress rapidly and generate metastases that remain the major cause of cancer-related mortality in these patients (Christofori, 2006). TNBC presents a major intratumoral heterogeneity that contributes to therapy failure and disease progression. The origin of this cellular heterogeneity is mainly explained by self-renewing breast cancer stem cells (CSCs) sustaining the long-term oligoclonal maintenance of the neoplasm (Kreso and Dick, 2014). We recently reported

[1]Division Hematology/Oncology, Department of Medicine, Feinberg School of Medicine, Northwestern University, Chicago, IL 60611, USA

[2]Explicyte, Cours de l'Argonne, 33000 Bordeaux, France

[3]CRCM, Inserm, CNRS, Institut Paoli-Calmettes, Aix-Marseille Univ, Epithelial Stem Cells and Cancer Lab, Equipe labellisée LIGUE contre le cancer, Marseille, France

[4]Department of Gynecology, University Hospital of Rennes, Rennes, France

[5]Centre Eugène Marquis, Rennes, France

[6]Department of Pharmacology, Feinberg School of Medicine, Northwestern University, Chicago, IL 60611, USA

[7]Department of Biochemistry and Molecular Genetics, Feinberg School of Medicine, Northwestern University, Chicago, IL 60611, USA

[8]Department of Biomedical Engineering, McCormick School of Engineering, Northwestern University, Evanston, IL, USA

[9]INSERM U1262, CRIBL, Université Limoges, Limoges, France

[10]These authors contributed equally

[11]Senior author

[12]Present address: Department of Pharmacology, The University of Illinois College of Medicine, Chicago, IL 60612, USA

[13]Lead contact

*Correspondence: m-peter@northwestern.edu (M.E.P.), patrick.legembre@inserm.fr (P.L.)

https://doi.org/10.1016/j.isci.2021.103348

that engaging CD95 on ER positive BC cells contributes to CSC survival (Qadir et al., 2017, 2020). Although CD95L-expressing immune cells edit tumor cells by sparing cancer cells expressing low CD95 level at their plasma membrane (Strasser et al., 2009), CD95 expression is high in TNBC cells (Blok et al., 2017), and the function of this receptor in these cancers remained unknown.

To examine the role of CD95 in a TNBC model, we generated two independent sets of CD95 knockout 4T1 clones using different methods and on different continents. Only in immune-competent mice, the deletion of CD95 caused a dramatic loss of tumor growth. This was accompanied by an increase in tumor-infiltrating T cells ($CD4^+$ and $CD8^+$ T cells) and natural killer (NK) cell and a reduction in granulocytic myeloid-derived suppressor cells (G-MDSCs), initially identified in human and mouse cancers due to their potent immunosuppressive activity (Marvel and Gabrilovich, 2015; Peranzoni et al., 2010). Depletion of myeloid cells, $CD8^+$, and $CD4^+$ T cells did not restore tumor growth of the CD95 k.o. cancer cells, whereas elimination of NK cells did. Our data point at a novel role of CD95 as a general immune suppressive receptor that advanced cancer cells maintain to avoid destruction by multiple immune cells, and more specifically, 4T1 tumor cells keep CD95 expression to prevent an NK-driven anti-tumor response.

RESULTS

Knock-out of CD95 does not affect the growth or stemness of 4T1 cells *in vitro*

We previously demonstrated that different cancers *in vivo* can barely grow without CD95 expression (Chen et al., 2010; Hadji et al., 2014). In contrast, knocking out CD95 in either ovarian cancer or a BC cell line did not substantially reduce growth of cancer cells *in vitro* (Putzbach et al., 2018). We were therefore wondering whether the tumor microenvironment and/or a functional immune system was required for CD95 expressing tumor cells to grow *in vivo* or whether they were responsible for the destruction of CD95-deficient tumor cells. Based on the results obtained with our genetically engineered mouse models (GEMMs) in which either tumors did not form or tumors that formed still expressed CD95 due to Cre recombination inefficiency, we concluded that this question could not conclusively be addressed in a CD95 k.o. GEMM. We therefore used CRISPR/Cas9 gene editing to delete CD95 in the aggressive murine TNBC cell line 4T1 that could be grown in syngeneic BALB/c mice (Aslakson and Miller, 1992). We generated single-cell clones with a complete biallelic knockout of CD95. To increase the rigor of the study and to eliminate any possibility of clonal effects or effects of Cas9 expression, two sets of k.o. clones were generated starting with different 4T1 lines and using different strategies to generate CD95 deficiency. The U-clones (generated in the US, all experiments in light blue boxes) involved the use of stable expression of GFP-Cas9 and a two-guide (sg)RNA system to delete exon 9 of murine CD95 (Figure S1A). On the other hand, the F-clones (generated in France, all experiments in light yellow boxes) were generated by transfecting both Cas9 and a sgRNA-plasmid, resulting in a frameshift mutation around the CD95 transcriptional start site (Figure S1B). Two U-clones were confirmed to not contain CD95-exon 9 anymore (Figure S1C). They had reduced total CD95 mRNA expression (Figure S1D), expressed little or no detectable CD95 on their cell surface (Figure S1E), and neither of the two k.o. clones had a consistent up- or downregulation of CD95L mRNA when compared with either parental cells or a Cas9 control clone (Figure S1F). Similarly, two k.o. F-clones were selected and expressed no detectable surface CD95 (Figure S1G). Similar to the human cell lines in which we had deleted CD95, none of the four 4T1 CD95 k.o. clones showed growth reduction *in vitro* or major cell-cycle changes when compared with their WT counterparts (Figures S1H–S1J).

We had recently reported for a number of ER^+ BC cell lines that chronic stimulation through CD95 induced cancer stemness through induction of a type I interferon response, which resulted in activation of STAT1 (Qadir et al., 2017, 2020). Stemness could also be increased by treating cells directly with type I interferons. In contrast, in the TNBC cell line 4T1 prolonged stimulation through CD95 or addition of IFNβ did not cause a substantial upregulation of CSC driving transcription factors, STAT1, or its major target gene PLSCR1 (Figure S2A). Although the stemness marker BMI1 was induced, the two E-box binding proteins ZEB1 and ZEB2 were not. Treatment of 4T1 cells with either LzCD95L or IFNβ also did not substantially affect cell growth (Figure S2B), and it did not increase the ability of the cells to form spheres (Figure S2C). It also did not result in an increase in ALDH1 activity (Figure S2D) or upregulation of CD44 (Figure S2E). Finally, treatment of 4T1 cells with LzCD95L did not induce a substantial amount of apoptosis (Figure S2F). These data suggest that the classical cell signaling pathways induced upon CD95 engagement are severely impaired in 4T1 cells despite the fact that these cells express substantial amounts of surface CD95. Although we did not see a significant and reproducible change in the expression of some of the stemness markers in the CD95 k.o. U-clones (Figure S2G), both CD95 k.o. U- and F-clones displayed a reduced ability

to form spheres when compared with control cells (Figures S2H and S2I). In summary, the stimulation of CD95 in 4T1 TNBC cells did not result in a major change in *in vitro* growth or cancer stemness, suggesting that CD95 on these cells has low signaling competence. On the other hand, although the stemness markers were not dramatically affected by CD95 loss in 4T1 cells, the loss of this receptor was associated with a slight but significant reduction in the ability of the cells to form spheres, suggesting that the presence of CD95 could alter some tumor features.

CD95-deficient 4T1 cells grow faster in immune-deficient mice than WT cells but do not form lung metastases

To determine whether the lack of CD95 expression would affect growth of 4T1 cells *in vivo*, we carried out an orthotopic graft of luciferase-expressing Cas9 control or a mixture of the two CD95 k.o. U-clones into the mammary fat pad of NSG mice (Figure 1A). After a lag phase of about 14 days, the k.o. U-cells grew more rapidly than WT cells in the immunocompromised NSG mice. When the two k.o. clones and the two WT controls were injected individually, tumor weight and volume were similar at two weeks in the mice (Figures 1B and 1C). The two F-k.o. clones generally grew more rapidly than WT cells (Figure 1D), suggesting that in immune-deficient mice, cells without CD95 had a growth advantage. This was not due to a difference in the expression of the stemness markers ALDH1 or CD44 (Figure 1E). NSG mice are devoid of lymphocytes and NK cells but do contain macrophages (Shultz et al., 2007). Although the number of intratumor myeloid-derived cells was the same in WT and k.o. tumors (Figure 1F), we observed a different distribution of F4/80 or CD163-expressing macrophages in CD95 k.o. compared with WT tumors (Figure S2J). Although F4/80- or CD163-expressing macrophages infiltrated WT tumors, these cells remained mostly at the periphery of CD95 k.o. tumors, pointing at a modulation of the immune landscape by tumor cells devoid of CD95 even in NSG mice.

4T1 cells are aggressively growing cancer cells that form lung metastases in implanted mice (Lelekakis et al., 1999). Although injection of WT 4T1 cells into NSG mice caused multiple lung metastases, barely any metastatic dissemination was detected in mice with implanted CD95 k.o. cells (Figures 1G and 1H). Interestingly, this occurred despite the fact that the primary CD95 k.o. tumors grew larger than the WT tumors in these mice. These data could be associated with the known activity of CD95 to increase motility and invasiveness of breast cancer cells (Barnhart et al., 2004; Malleter et al., 2013) and could also be related to the reduced capacity of CD95-deficient 4T1 cells to form spheroids compared with WT counterparts (Figures S2H and S2I).

CD95-deficient 4T1 cells barely grow in immune-competent mice compared with WT cells and show reduced markers of stemness

We next wondered whether the loss of CD95 by tumor cells could impair tumor growth by modulating immune infiltrates. To evaluate this possibility, we orthotopically grafted 4T1 cells into syngeneic BALB/c mice. CD95 k.o. 4T1 cells grew much less than WT cells, which only stopped growing when reaching a certain size and becoming necrotic (Figure 1I). To exclude an immune effect linked to the fact that CD95 WT and U-k.o. clones expressed the xeno-antigen luciferase (Baklaushev et al., 2017), we performed the experiment with unlabeled parental cells and compared the growth of parental cells with that of the vCas9 and the two CD95 k.o. U-clones individually (Figures 1J and 1K). Tumors were harvested after two weeks of growth in the mice. Consistent with the above results, both the parental and unmodified 4T1 cells as well as the Cas9 expressing WT cells grew much faster than the CD95 k.o. clones as monitored by both tumor volume and tumor weight (Figures 1J and 1K). In fact, the CD95 k.o. cells barely grew in these mice. This behavior of CD95 k.o. cells was largely confirmed by the orthotopic xenograft of the F-clones into BALB/c mice (Figure 1L). Tumor growth of the two k.o. clones was less efficient than that of the parental cells or of a WT clone. In contrast to the tumors grown in NSG mice, *ex vivo* isolated CD95 k.o. U-clone tumor cells from the BALB/c mice showed a clear reduction of the stemness markers ALDH1 and CD44 when compared with WT tumors (Figure 1M), suggesting that the immune system regulated the survival of CSCs in CD95 k.o. cells. Unexpectedly, these data indicated that the loss of the death receptor CD95 reduces tumor growth only in mice that have a functional immune system.

Gene expression analysis identifies a general immune activation inside the CD95 k.o. tumors in immune-competent mice

To get insights into what is causing the suppression of tumor growth after CD95 deletion in TNBC cells, we subjected two 4T1 WT controls (WT and vCas9 expressing) and the two CD95 k.o. U-clones to an RNAseq

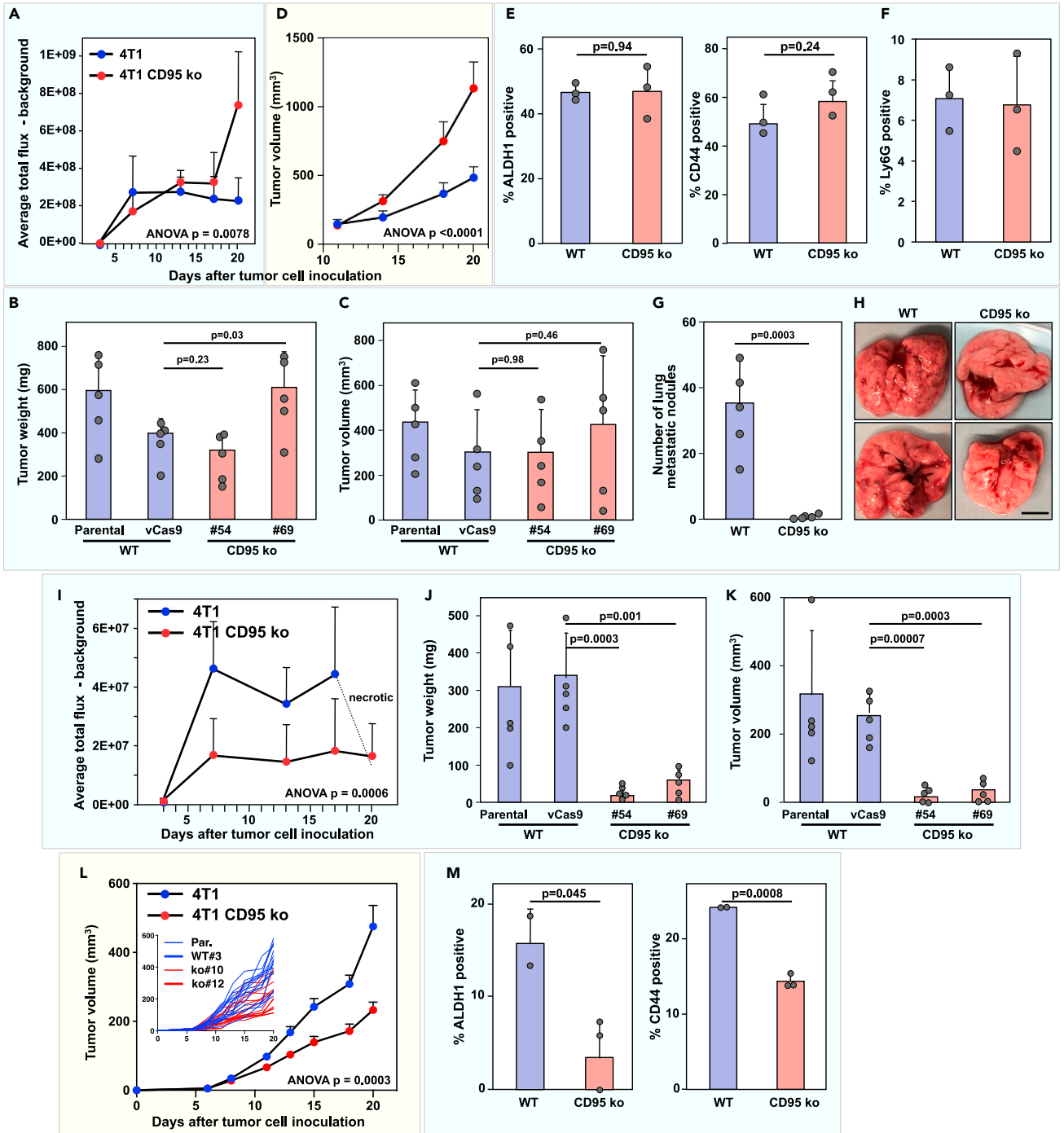

Figure 1. Deletion of CD95 in 4T1 cells inhibits tumor growth and cancer stemness in BALB/c mice but not in NSG mice

(A) Wild-type (vCas9) or CD95 k.o. 4T1 (mixture of clones #54 and #69) cells (10^5) were injected into the fat pad of NSG mice. Bioluminescence of tumors was quantified at the indicated times after injection of cells.

(B and C) Equal numbers of WT (Parental or vCas9) or CD95 k.o. (#54 or #69) 4T1 cells were transplanted into the mammary fat pad of NSG mice, and tumor weight (B) and tumor volume (C) were measured after two weeks.

(D) Wild-type (mixture of clones #3 and #4) or CD95 k.o. 4T1 (mixture of clones #10 and #12) cells (10^5) were injected into the mammary fat pad of NSG mice, and tumor volume was measured using a caliper.

(E) ALDH1 activity and CD44 surface staining of single-cell suspensions of tumors isolated from NSG mice. n = 3 for each group.

(F) IHC quantification of Ly6G positive cells in the WT and CD95 k.o. tumors monitored in (B). n = 3 biological replicates.

Figure 1. *Continued*

(G) Equal numbers of WT (Parental or vCas9) or CD95 k.o. (1:1 mixture of #54 or #69) 4T1 cells were transplanted into the mammary fat pad of NSG mice, and tumor nodules of the primary tumor on the surface of the lungs were counted two weeks after transplantation.

(H) The appearance of representative lungs analyzed in (G). Scale bar, 5 mm.

(I) Luciferase expressing wild-type (cCas9) or CD95 k.o. 4T1 (mixture of two k.o. clones) cells (10^5) were injected into the mammary fat pad of BALB/c mice. Bioluminescence of tumors was quantified at the indicated times after injection of cells.

(J and K) Equal numbers of unmodified WT (Parental or vCas9) or CD95 k.o. (#54 or #69) 4T1 cells were transplanted into the mammary fat pad of BALB/c mice, and tumor weight (J) and tumor volume (K) was measured after two weeks.

(L) Parental, WT (#3) and two CD95 k.o. (#10 and #12) 4T1 cells (10^5 cells) were injected into the mammary fat pad of BALB/c mice (n = 8), and tumor volume was measured using a caliper. Insert shows the growth of the individual tumors.

(M) ALDH1 activity and CD44 surface staining of single-cell suspensions of tumors isolated from BALB/c mice. WT n = 2, k.o. n = 3, biological replicates. Representative data from two independent experiments.

Experiments involving U-clones (n = 5, unless otherwise defined) are in a light blue box and experiments involving F-clones (n = 10) are in a light yellow box, respectively. Data are shown as the mean ± SD. p value was calculated using two-way ANOVA (A, D, I, and L) or two-tailed Student's t test (B, C, E–G, J, K, and M). See also Figures S1 and S2 and Table S1.

analysis under three different conditions: cells grown *in vitro*, cells grown in NSG, and cells grown in BALB/c mice. As the goal was to identify genes with altered expression in the tumors between WT and k.o. tumor specifically in the BALB/c mice, we performed a differential gene expression analysis using DESeq2 (Figure S3). The number of significantly expressed genes across all samples was 13,083, and the numbers of genes differentially expressed (padj <0.05) between WT and k.o. cells was 496 (cell lines), 485 (NSG mice), and 620 (BALB/c mice). This amounted to 1,090 differentially expressed unique genes. We performed k-means clustering with 6 clusters (determined by elbow plot) and plotted a heatmap of adjusted expression to identify trends and unique groups (Figure S3A). The most significant GO terms are listed for each cluster. Genes in the top two clusters were most highly deregulated specifically in the tumors grown in BALB/c mice when compared with either *in vitro* grown cells or grown in NSG mice. Genes in cluster 1 were upregulated in the CD95 k.o. tumors and genes in cluster 2 were downregulated. These changes could be caused either by gene expression changes in the tumor cells or more likely by infiltrating immune cells. Most importantly, due to the way the data were analyzed these changes did not reflect the difference between NSG and BALB/c mice but rather the difference between WT and CD95 k.o. tumors in the context of immune-competent mice. To identify the function of the most highly deregulated genes, we ranked all deregulated genes across all 6 clusters according to the greatest fold difference in the k.o./WT ratio between BALB/c compared with NSG mice and subjected this list to a GO analysis (Figure S3B). Ten of the twenty-two most significantly enriched GOs in the BALB/c mouse tumors were related to immune function and activation of specific immune cell subsets. These results pointed at a general increase in immune cell infiltration and activity in tumors lacking CD95.

Deletion of CD95 in TNBC cells causes a modulation of the immune landscape

Based on the results of the differential gene expression analysis of CD95 k.o. cells, we subjected U-clones grown as tumors in BALB/c mice to immunohistochemistry analysis (Figure 2A). Macrophages (F4/80 staining) were found mostly at the periphery of the tumors, and they were more abundant in CD95 k.o. tumors (Figure 2B). T cells ($CD4^+$, $CD8^+$, and regulatory T cells [Tregs—FOXP3 staining]) infiltrated k.o. tumors more readily compared with WT tumors (Figures 2A and 2B). This was pronounced for $CD8^+$ T cells that were abundant and showed the most homogeneous staining inside the CD95 k.o. tumors, whereas very few $CD8^+$ T cells were detected inside WT tumors (Figures 2A and 2B). Tumor vessel density (CD31 staining) was similar between WT and k.o. tumors (Figures 2A and 2B). These results suggested that CD95 expression in cancer cells could prevent immune cells including cytotoxic killer cells from infiltrating the tumors but had no effect on tumor vascularization, at least not in this rapidly growing tumor model. The IHC analysis of the U-tumors was followed up by a detailed multi-parameter flow cytometry analysis of the tumor infiltrate inside the F-clones grown in BALB/c mice (Figure 2C). In agreement with the U-clone results, this analysis confirmed that a large number of different immune cells had preferentially infiltrated the CD95 k.o. tumors, including macrophages ($CD45^+CD11b^+F4/80^+$), both M1 ($CD45^+CD11b^+F4/80^+CD38^+$) and M2 ($CD45^+CD11b^+F4/80^+CD38^-$) macrophages (Jablonski et al., 2015), and all types of T cells as evidenced by an increase in $CD3^+$, $CD4^+$, and $CD8^+$ cells (Figure 2C). MDSCs are a heterogeneous population of immature myeloid cells that include monocytic (M-MDSC, $CD45^+CD11b^+Gr1^{High}Ly6C^{High}$) and granulocytic (G-MDSC, $CD45^+CD11b^+Gr1^{High}Ly6G^+$) subsets, both of which have been shown to exert immune-suppressive activities. Within tumors, additional myeloid cells referred to as tumor-associated macrophages (TAM) display immunosuppressive activity (Ugel et al., 2015). Although the number

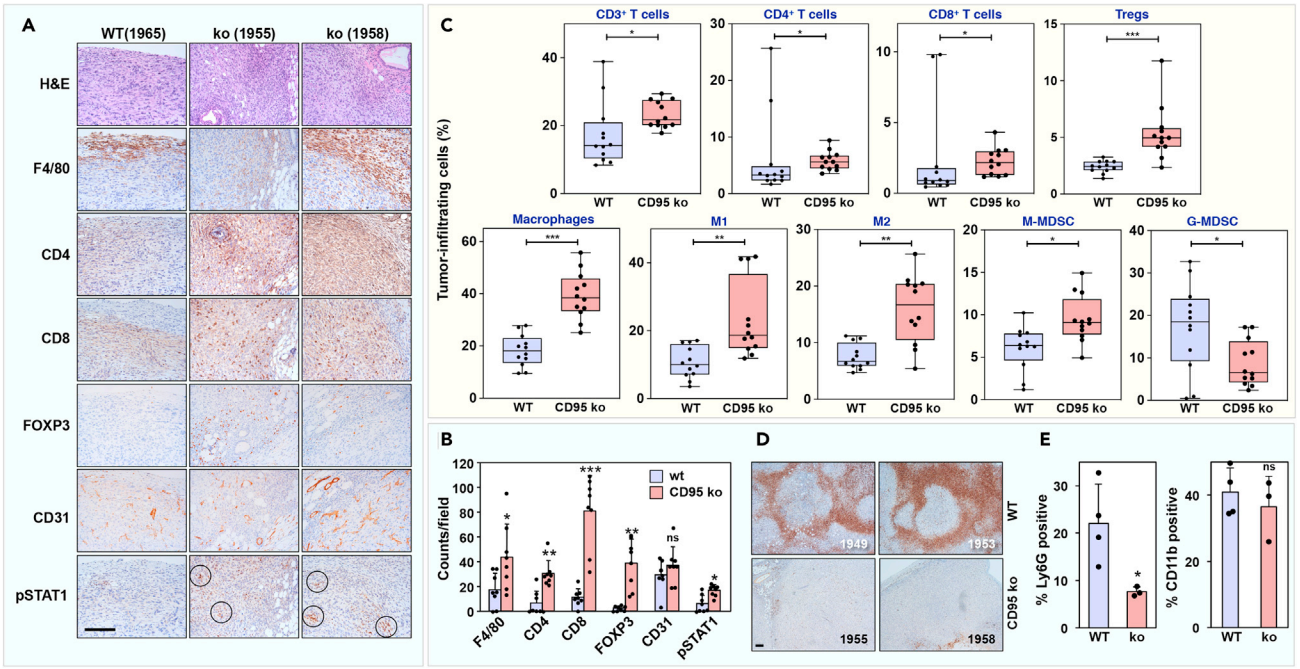

Figure 2. CD95 loss in TNBC cells increases general immune cell infiltration with only G-MDSCs being reduced when compared with WT tumors

(A) WT or CD95 k.o. 4T1 cells were injected into the mammary fat pad of BALB/c mice. Mice were sacrificed when tumors reached maximum allowed size or signs of ulceration were evident. Representative tumor sections of one mouse grafted with WT (1965) and two mice grafted with k.o. cancer cells (1955, 1958) stained with hematoxylin and eosin (H&E) or with antibody specific for mouse macrophages (F4/80), T cells (CD4, CD8, FOXP3), endothelial cells (CD31), or pSTAT1. Representative images of the immunohistochemical analysis and H&E staining are shown. Black circles highlight pSTAT1 positive cell clusters.

(B) The staining intensity of F4/80, CD4, CD8, FOXP3, pSTAT1, and CD31 was quantified. (biological replicates, $n = 8$).

(C) After 21 days, tumors grown in Figure 1L were resected and dissociated. Tumor-infiltrating cells including macrophages ($CD45^+CD11b^+F4/80^+$); whole $CD3^+$ T cell population, $CD3^+CD4^+$, $CD3^+CD8^+$ T cells, and Treg ($CD3^+CD4^+CD25^{High}FoxP3^+$) subsets; M1 ($CD45^+CD11b^+F4/80^+CD38^+$) and M2 ($CD45^+CD11b^+F4/80^+CD38^-$); and M-MDSC ($CD45^+CD11b^+Ly6C^+Ly6G$) and G-MDCS ($CD45^+CD11b^+Ly6C^{Low}Ly6G^+$) were quantified by multiparameter flow cytometry with the indicated combination of markers. n = 12 biological replicates. Central band is the median, and the whiskers define the minimum and maximum values. Nonparametric Mann-Whitney test p value shown.

(D) Representative tumor sections of two mice injected with WT (1953, 1949) and two mice injected with k.o. cancer cells (1955, 1958) stained for Ly6G.

(E) IHC quantification of Ly6G positive cells (left, examples shown in (D)) and CD11b (right) in the WT and CD95 k.o. tumors analyzed in (B). WT n = 4, k.o. n = 3 biological replicates.

Mean ± SD, two-tailed Student's t test. p value shown (B and E), p value *<0.05, **<0.001; ***<0.0001; ns, not significant. Scale bars, 50 μm. See also Figure S3.

of M-MDSCs was increased, the number of G-MDSCs was reduced in the k.o. tumors (Figure 2C). To independently confirm this finding, we stained the U-clone tumors for Ly6G to detect G-MDSCs and confirmed the staining to be strongly reduced in the k.o. tumors (Figures 2D and 2E, left panel), whereas the general macrophage marker CD11b was unchanged (Figure 2E, right panel). These findings indicated that in TNBC cells, CD95 expression can impinge on the trafficking of many cytotoxic immune cells including $CD8^+$ T cells into the tumor tissue.

$CD8^+$ T cells are not responsible for the reduced growth of CD95 k.o. tumors

Studies have shown that tumor infiltrating lymphocytes (TILs) have a strong prognostic impact on women affected by TNBC (Ali et al., 2014, 2016). A major reduction in disease and distant recurrences was reported for TNBC patients having high amounts of TILs (Ibrahim et al., 2014). We first tested to what degree infiltrating $CD8^+$ T cells detected in the k.o. tumors were responsible for the reduced tumor growth. To address this question, we depleted $CD8^+$ T cells in BALB/c mice by repeated injection of a neutralizing anti-CD8 mAb (Figure 3A). Staining for $CD8^+$ T cells in the spleen of depleted mice was undetectable, whereas that of $CD4^+$ T cells remained unaffected (Figures 3B and 3C). 4T1 cells (U-clones) when grown *in vivo* resulted in a substantial increase in spleen size and weight compared with CD95 k.o. counterparts (Figure 3D). Of note, the reduced growth of CD95 k.o. cells compared with WT cells *in vivo* was not affected by the $CD8^+$

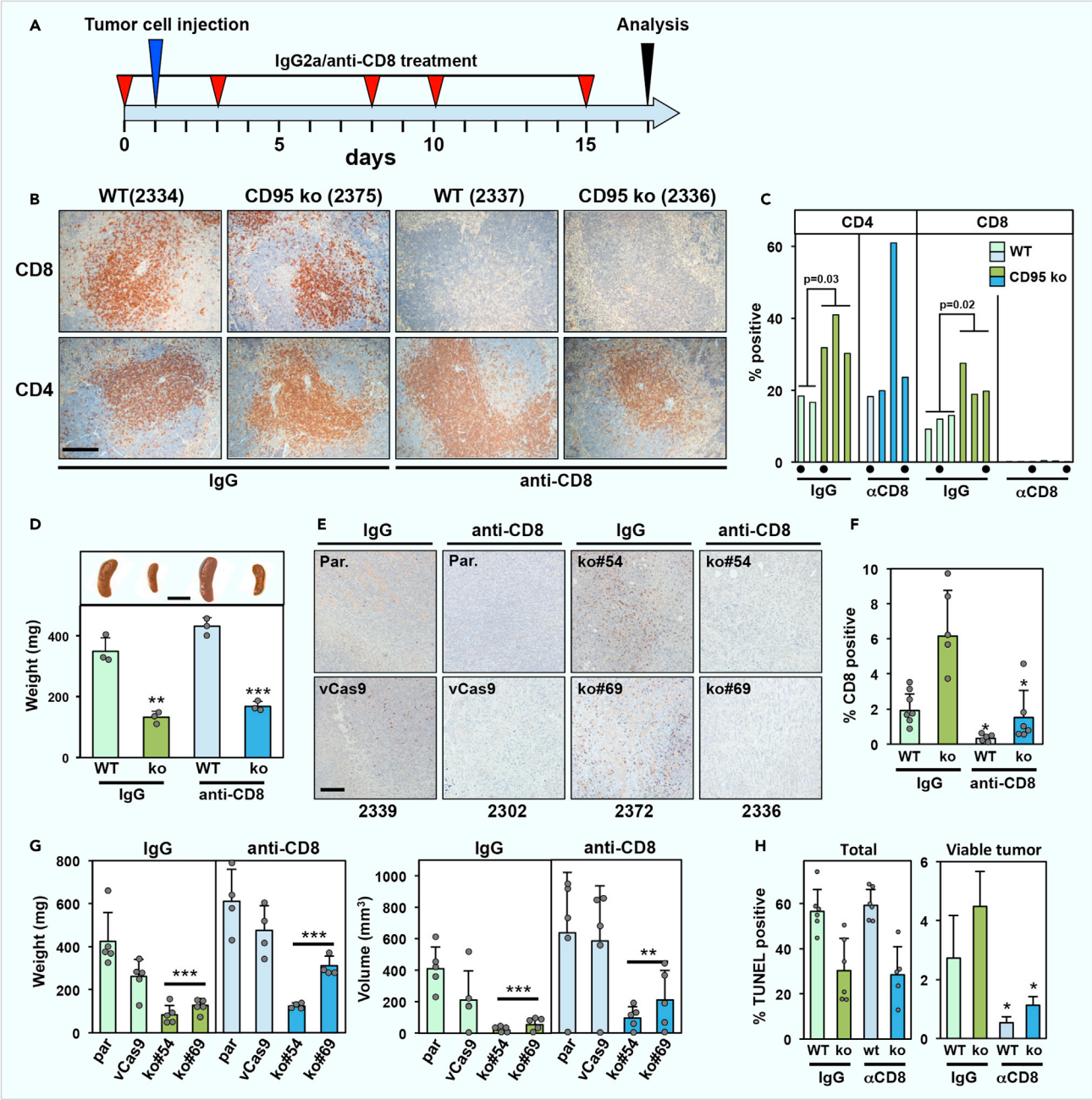

Figure 3. CD8⁺ T cells are not critical for the anti-tumor response against CD95 k.o. cells

(A) Treatment scheme of BALB/c mice with implanted WT or CD95 k.o. cells and treated with control or anti-CD8 antibody.

(B) Representative IHC images of spleens from mice treated with either isotype matched control antibody or anti-CD8 as indicated and stained for $CD4^+$ or $CD8^+$ T cells. Scale bar, 50 μm.

(C) Quantification of CD4 and CD8 T cells in the spleen of mice treated with either IgG or anti-CD8. Values labeled by a dot correspond to the images shown in (B).

(D) (*Top*) Representative images of spleens of treated mice. (*Bottom*) Average spleen weight of treated mice (n = 3). Scale bar, 1 cm.

(E) IHC of WT or CD95 k.o. tumors grown in BALB/c mice after depletion of $CD8^+$ T cells staining with anti-CD8 mAb. Mouse numbers are shown below. Experiments were performed with the U-clones. Scale bar, 50 μm.

(F) Quantification of CD8 T cells in tumors (n = 5–6) of mice treated with either IgG or anti-CD8 mAb.

(G) Tumor weight (left) and tumor volume (right) in anti-CD8-treated mice (n = 5) 16 days after tumor injection.

(H) IHC quantification of TUNEL staining of sections of WT and k.o. tumors in mice (n = 6) treated as in (G).

Shown are the mean ± SD. p value was calculated using two-tailed Student's t-test. p value *<0.05; **<0.001; ***<0.0001.

T cell depletion despite the fact that CD8 infiltration was dramatically reduced in the CD95 k.o. tumors upon CD8 depletion (Figures 3E and 3F). CD8 depletion had some effect on tumor growth, as both WT and k.o. tumors grew slightly larger in the depleted mice (Figure 3G). Although the amount of cell death in the total tumor was not affected by the $CD8^+$ T cell depletion (Figure 3H, left panel), when areas of the tumors were analyzed that did not show overt cell death or necrosis (viable tumor tissue), $CD8^+$ T-cell-depleted tumors (both CD95 k.o. and WT 4T1 cells) experienced less TUNEL staining than untreated tumors; however, no difference was observed in fold change between CD95 k.o. and WT tumors (Figure 3H, right panel). These data suggested that although $CD8^+$ T cells control tumor growth of the 4T1 cells in general, the increased CTL infiltration observed into the CD95 k.o. tumors (Figures 2A, 2B, and 2C) did not explain the strongly reduced tumor growth after deletion of CD95.

Neither $CD4^+$ T cells nor myeloid cells are responsible for the reduced growth of CD95 k.o. tumors

Similar to CD8 T cells, depletion of $CD4^+$ T cells did not exhibit a stronger anti-tumor effect on the reduced growth of CD95 k.o. tumors compared with the parental counterparts (Figures S4A–S4C), suggesting that tumor-infiltrating T cells were not responsible for the selective antitumor activity observed in CD95 k.o. tumors. Because of the differences in the amounts of M-MDSCs and TAM observed in WT and k.o. tumors (Figure 2C), we treated mice with an antibody to neutralize CSF1-R, which has been shown to prevent the recruitment of tumor-infiltrating myeloid cells including TAM and M-MDSCs (Priceman et al., 2010; Ries et al., 2014) (Figure S4D). This experiment was also carried out because among all the CSF ligand and CSF receptor genes in our differential gene expression analysis, CSF1-R was the most highly deregulated gene between the two CD95 k.o. clones and the WT cells, both *in vitro* and when grown as tumors in BALB/c mice (but not in NSG mice) (Table S1). Targeting CSF1-R had no effect on tumor growth of either WT or CD95 k.o. tumors despite this antibody treatment leading to a decrease in TAMs and M-MDSCs and an increase in $CD4^+$ and $CD8^+$ T cells (Figures S4E–S4G).

NK cells are involved in the antitumor response against CD95-deficient TNBC cells

Finally, to test whether NK cells could be responsible for the reduced growth of CD95 k.o. tumors in BALB/c mice, we compared side-by-side the growth of WT and k.o. tumors in NOD-SCID IL2Rgamma^{null} (NSG), NOD-SCID, and BALB/c mice. Although both NSG and NOD-SCID mice have normal macrophages and are both C5 complement deficient (Baxter and Cooke, 1993; Serreze, 1993), NOD-SCID mice differ from their NSG counterparts mainly in the presence of NK cells (Presa et al., 2015; Shultz et al., 2012). Interestingly, the reduced tumor growth of the CD95 k.o. cells in NOD-SCID mice was similar to the one seen in the immunocompetent BALB/c mice and reversed to the situation in NSG mice (Figure 4A). Consistent with this finding, CD95 k.o. tumors exhibited a significantly higher number of tumor-infiltrating NK cells as compared with WT tumors in NOD-SCID mice (Figure 4B). To confirm the anti-tumor activity of NK cells in CD95-k.o. cancers, we depleted NK cells in BALB/c mice by repeated injections of an anti-Asialo GM1 Ab (Figures 4C and 4D). Strikingly the NK depletion significantly minimized the growth difference of primary tumors between WT and k.o. cells (Figures 4E and 4F).

In summary, our data suggest that the expression of CD95 on tumor cells regulates the global immune landscape, and the anti-tumor activity of NK cells can be stimulated by the loss of CD95 in TNBC cells.

DISCUSSION

We previously reported that deletion of CD95 *in vivo* strongly reduced tumor formation and growth in three different mouse tumor models (Chen et al., 2010; Hadji et al., 2014). In all cases, endogenous CD95 was deleted using Cre recombinase. In two of these models, one involving DEN-induced liver cancer and one low-grade ovarian cancer, we determined that most, if not all, tumor nodules that grew in these CD95 k.o. mice still expressed CD95 (Chen et al., 2010; Hadji et al., 2014) due to inefficient deletion by Cre. In this study, we therefore used a syngeneic orthotopic cell line model that allowed us to selectively and completely delete CD95 in all cancer cells and assess its effect on tumor growth in immune-competent mice. We chose BC as a model because we had previously identified CD95 as a driver of cancer stemness in the context of BC (Ceppi et al., 2014; Qadir et al., 2017, 2020). We found that although the loss of CD95 in TNBC cells did not substantially affect cancer cell survival in an immune-depressed mouse model, when introduced into immune-competent mice, CD95 k.o. tumors barely grew.

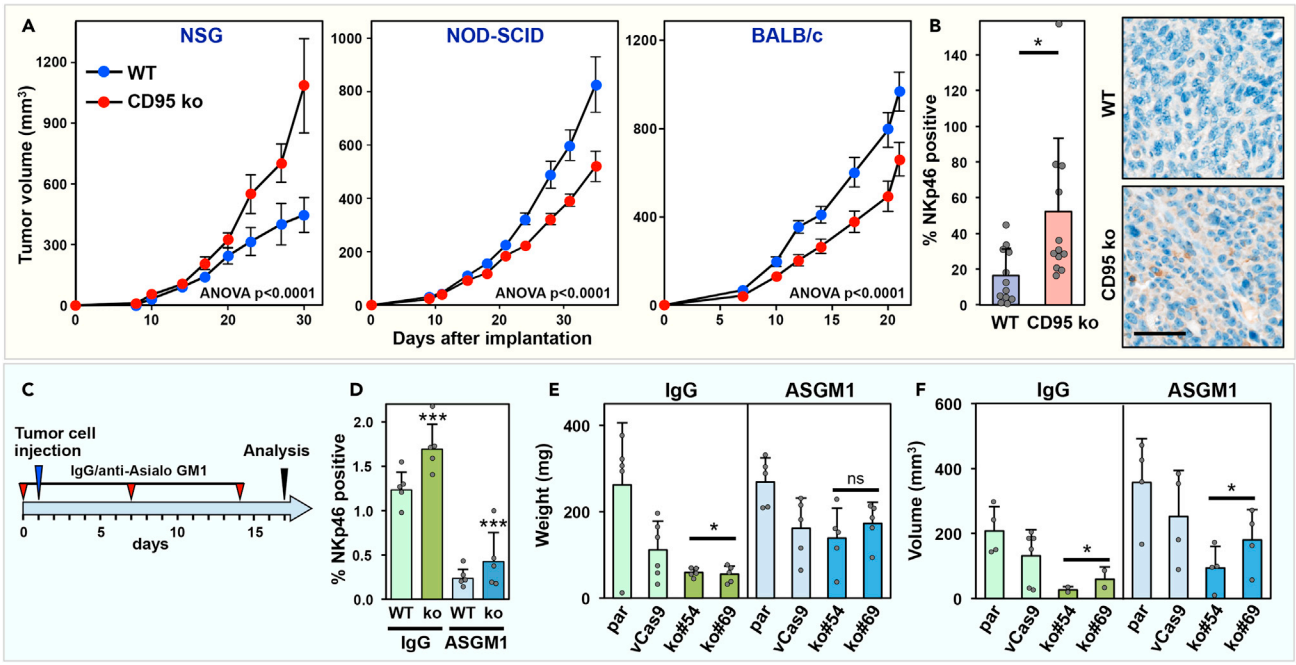

Figure 4. NK cells are involved in attacking CD95 k.o. tumor cells in BALB/c mice

(A) Tumor growth of a mix of WT 4T1 cells and a CD95 k.o. clone #4 in three different mouse strains (n = 8). p values were calculated using two-way ANOVA.

(B) (*Left*) IHC quantification of NKp46-positive NK cells (cells/mm^2) in WT and CD95 k.o. tumors grown in NOD-SCID mice shown in (A). (*Right*) Representative images of a WT and CD95 k.o. tumor stained for NKp46. p value was calculated using nonparametric Mann-Whitney test (in 3 different tumors, NK cells were counted on 4 different fields). Scale bar, 50 μm.

(C) Treatment scheme of BALB/c mice with implanted WT or CD95 k.o. cells and treated with control or anti-Asialo GM1 antibody.

(D) Quantification of NKp46 positive NK cells in the spleen of mice treated with either IgG or anti-Asialo GM1 (n = 5).

(E and F) Tumor weight (E) and tumor volume (F) in anti-Asialo GM1-treated mice (n = 5) 16 days after tumor injection.

Mean ± SD, two-tailed Student's t test (D–F). p value *<0.05; ***<0.0001. ns, not significant. See also Figure S4.

A recent analysis of a cohort of 667 BC patients revealed that CD95 expression increases with advancing grade of disease (Blok et al., 2017). In fact, ER-negative BC including TNBCs had almost twice as much CD95 expression as ER-positive BC. The TNBC 4T1 cell line is part of a series of five BC cell lines that were isolated from mice after sequential growth and differ in their metastatic potential (Miller et al., 1983). 4T1 is the most aggressive of these cell lines. Consistent with the data on human TNBC, 4T1 cells have very high expression of CD95.

Our differential analysis of genes upregulated in the k.o. tumors suggested a fundamental recruitment of immune cells with antitumor activity. The decreased recruitment of G-MDSCs together with the increase in CD8$^+$ T and NK cells in the CD95 k.o. tumors we then observed left two possibilities to explain the dependence of tumor cells on CD95 to grow *in vivo*: (1) WT tumors grow more because MDSCs are generating an immunosuppressive environment or (2) the reduced growth of CD95 k.o. tumors might be due to an increased recruitment of TILs. Interestingly, our findings are in agreement with previous reports showing that although G- and M-MDSCs promote the metastatic dissemination of 4T1 TNBC cells (Ouzounova et al., 2017; Youn et al., 2008), their elimination by CSF1-R-targeting treatments does not affect primary tumor growth (Swierczak et al., 2014). A good prognostic score was shown to be associated with CD8$^+$ TILs in ER-negative disease with high CD95 expression (Blok et al., 2017), suggesting that CTLs attack high CD95-expressing tumor cells. However, we now demonstrate that although CD8$^+$ CTLs exert a general anti-tumor effect in the 4T1 model, the loss of CD95 in TNBC cells engenders an anti-tumor response through the recruitment and activation of NK cells. This finding is consistent with a report showing that treatment of mice with IL-21, a cytokine involved in the NK cell proliferation and activation (Parrish-Novak et al., 2000), enhances 4T1 tumor rejection (Takaki et al., 2005). Not much is known about the role of NK cells in TNBC, but molecular signatures associated with NK cells have been shown to be predictive of relapse-free survival in BC patients including TNBC patients (Ascierto et al., 2013).

We can now separate different observations on the apoptosis-independent and cancer-relevant functions of CD95 into at least four activities. (1) CD95 drives metastasis formation in a cell autonomous fashion. This observation is supported by multiple reports demonstrating increased motility or invasiveness of tumor cells upon CD95 stimulation (Barnhart et al., 2004; Briggs et al., 2017; Cai et al., 2012; Hoogwater et al., 2010; Kleber et al., 2008; Letellier et al., 2010; Lin et al., 2012; Liu et al., 2014; Malleter et al., 2013; Teodorczyk et al., 2015; Trauzold et al., 2005; Zheng et al., 2013). Interestingly, we found that in NSG mice, 4T1 cells only form metastases when CD95 is expressed, suggesting that it is indeed a metastatic driver. (2) Stimulation of CD95 on cancer cells increases their proliferation. We reported evidence of increased CD95 driven proliferation of cancer cells and in fact stimulating apoptosis-resistant cancer cells through CD95 increases their growth rate (Li et al., 2009; Mapara et al., 1993; Putzbach et al., 2017). (3) CD95 stimulation increases cancer stemness (Ceppi et al., 2014; Drachsler et al., 2016). We previously showed that chronic stimulation of CD95 on multiple cancer cell lines including ER^+ BC induces production of type I interferons, which through activation of type I IFN receptors and activation of STAT1 drives cancer stemness (Qadir et al., 2017, 2020). (4) In the present study, we uncover a novel and unexpected activity of CD95 as an immune suppressive receptor that when expressed on tumor cells prevents infiltration of multiple immune cells into the tumor.

We do not believe that the finding on the role of CD95 as a suppressor of tumor immune infiltration is limited to the 4T1 TNBC model. Our data provide an explanation for a long-standing enigma of why in GEMMs of endometrioid, low-grade ovarian cancer, or liver cancer tumors could not efficiently grow *in vivo* after knock-out of CD95 (Chen et al., 2010; Hadji et al., 2014). In addition, in the model of low-grade ovarian cancer, we noticed that the deletion of CD95 in the tumors in the ovaries led to a massive amount of hemorrhage, necrotic cell death, and an increase in infiltration of proinflammatory immune cells (Hadji et al., 2014). We had interpreted this result as a requirement for CD95 for the cancer cells to survive but in this mouse model, we could not determine whether the increase in inflammation we observed was the cause or the consequence of dying tumor cells. Our data now suggest that the deletion of CD95 on the developing tumor cells triggered massive trafficking of immune cells. Nonetheless, further investigations are required to definitively establish that maintaining CD95 expression in cancer cells is a general mechanism to prevent NK-mediated antitumor activity.

Although CD95 stimulation is not required for the destruction of the tumor by NK cells as it only occurs after homozygous deletion of CD95 in the tumor cells, it is currently unknown whether CD95L is required for the immune suppressive activities of CD95. The inability of 4T1 cells to significantly respond to even prolonged CD95 stimulation suggests an activity of CD95 that is independent of its stimulation by CD95L. This conclusion is also supported by our companion study demonstrating that deletion of CD95 in both human and mouse TNBC cells resulted in NF-κB activation and the secretion of proinflammatory chemo- and cytokines (Guegan et al., 2021). Mechanistically we identified KPC2 as a novel CD95 interaction partner that binds to CD95's C-terminal end and in unstimulated TNBC cells sequesters both the NF-κB subunit p65 and KPC1, a ubiquitin ligase that degrades the p50 precursor p105 (Kravtsova-Ivantsiv et al., 2015). We showed that when CD95 is lost, p105 gets degraded shifting the balance of NF-κB subunits from repressive p50/p50 homodimers to transcriptionally active p50/p65 heterodimers. That in turn unleashes the production of inflammatory cytokines, regulating the recruitment of a number of immune cells including NK cells.

We can exclude 4T1 cells as a source of CD95L, as they do not express CD95L (Sinha et al., 2011), and the activation of NF-κB did not occur after deletion of the CD95L gene (Guegan et al., 2021). Our data therefore provide support of the idea not only to target CD95L to block the tumorpromoting activities of CD95L (Wick et al., 2014, 2019a, 2019b) but also to target the CD95 receptor directly.

In summary, this study reveals that CD95 expression on tumor cells impairs the immune attack and when removed enhances the destruction of tumors by the immune system (Figure 5), suggesting that CD95 is an immune checkpoint regulator, and the generation of CD95-targeting antagonists could mimic or add to the therapeutic effects of established checkpoint inhibitors.

Limitations of the study

CD95 has been shown to have many tumor promoting activities. Our new data now raise the question of how this new activity contributes to or interferes with these established activities. In general, it needs to be tested in what cancers or breast cancer subtypes CD95 acts as an immune suppressor. We cannot

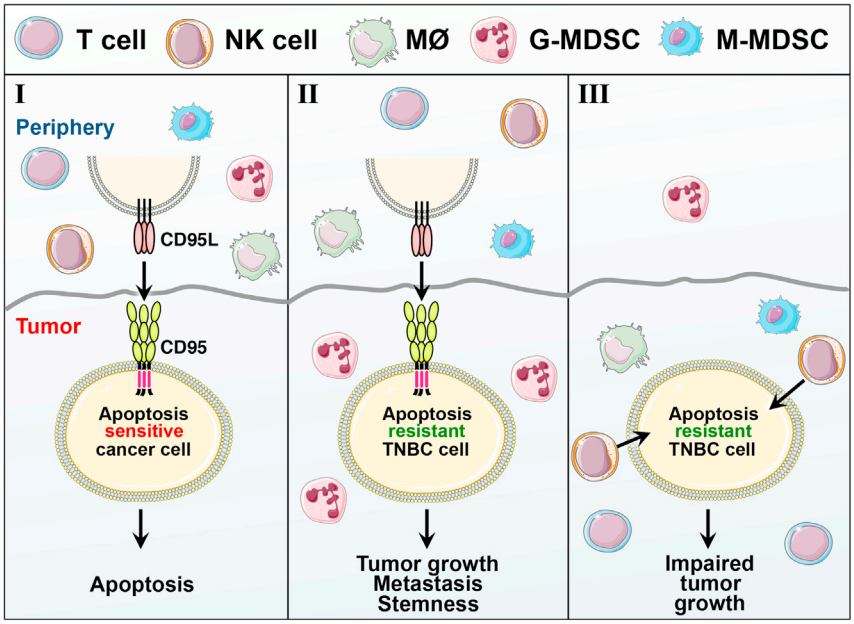

Figure 5. Model to illustrate the novel activity of CD95 as an immune suppressor in TNBC

In addition to its well-established function as an apoptosis inducing receptor (I), CD95 has multiple nonapoptotic activities. When apoptosis-resistant tumor cells are exposed to CD95L, this causes increased tumor growth, cancer stemness, or metastasis (II). In TNBC cells where it is highly expressed, deletion of CD95 results in an increase of tumor infiltrating immune cells and in the 4T1 model in tumor destruction by NK cells.

exclude that in other cancers immune cells other than NK cells are involved in the tumor attack. Because the activity of CD95 manifests when CD95 is deleted from the tumor cells, stimulation of CD95 by CD95L is likely not involved in the immune destruction. Although we cannot exclude that CD95L stimulation of wild-type cells triggers a signaling program in the tumor that suppresses immune infiltration, our companion manuscript (Guegan et al., 2021) rather suggests that this activity does not involve CD95L.

STAR★METHODS

Detailed methods are provided in the online version of this paper and include the following:

- KEY RESOURCES TABLE
- RESOURCE AVAILABILITY
  - Lead contact
  - Materials availability
  - Data and code availability
- EXPERIMENTAL MODEL AND SUBJECT DETAILS
  - Cell lines
  - Animal studies
  - Growth of 4T1 cells in NGS and Balb/c mice
- METHOD DETAILS
  - Reagents
  - CRISPR/Cas9 mediated deletion of CD95
  - FACS analysis
  - Sphere forming assays
  - Cell growth/Proliferation assay
  - Cell death assays and cell cycle analysis
  - Real-time PCR
  - Depletion of immune cells in mice
  - Immunohistochemistry analysis
  - IHC quantification

- RNA-seq library construction from cell lLines grown *in vitro*
- RNA-seq library construction from tumors grown *in vivo*
- RNA-seq and gene ontology data analysis

- QUANTIFICATION AND STATISTICAL ANALYSIS
- ADDITIONAL RESOURCES

SUPPLEMENTAL INFORMATION

Supplemental information can be found online at https://doi.org/10.1016/j.isci.2021.103348.

ACKNOWLEDGMENT

U-clones: we would like to thank Shanshan Zhang for performing slide scanning and signal quantification, Michelle von Locquenghien for help with the generation of the 4T1 CD95 k.o. clones, and Bin Zhang for giving advice. F-clones: we would like to thank the IHC facility (Dr. Alain Fautrel and Roselyne Viel, Rennes, France) for performing 4T1 tissue staining, slide scanning, and signal quantification. The mouse study in NSG mice benefited from the help of Remy Castellano and Emmanuelle Josselin (Marseille, France). This work was funded by grant R35CA197450 to M.E.P, by INCa (PLBIO18-059), Ligue Contre le Cancer and Fondation de France (Price Jean Valade) for P.L., and by Lynn Sage Cancer Research Foundation and Lynn Sage Scholar fund for Z.J.

AUTHOR CONTRIBUTIONS

ASQ, JPG, CG, EC-J, AB, VL, TMR, PL, ZJ, and MEP planned the experiments. ASQ, JPG, CL, HW, ES, AC, JV, MJS, MM, AEM, and BB performed experiments or analyzed data. PL and MEP directed the study and wrote the manuscript.

DECLARATION OF INTERESTS

The authors declare that they have no conflict of interest.

Received: June 21, 2021
Revised: October 12, 2021
Accepted: October 22, 2021
Published: November 19, 2021

REFERENCES

Algeciras-Schimnich, A., Shen, L., Barnhart, B.C., Murmann, A.E., Burkhardt, J.K., and Peter, M.E. (2002). Molecular ordering of the initial signaling events of CD95. Mol. Cell. Biol. *22*, 207–220.

Ali, H.R., Provenzano, E., Dawson, S.J., Blows, F.M., Liu, B., Shah, M., Earl, H.M., Poole, C.J., Hiller, L., Dunn, J.A., et al. (2014). Association between CD8+ T-cell infiltration and breast cancer survival in 12 439 patients. Ann. Oncol. https://doi.org/10.1093/annonc/mdu191.

Ali, H.R., Chlon, L., Pharoah, P.D., Markowetz, F., and Caldas, C. (2016). Patterns of immune infiltration in breast cancer and their clinical implications: a gene-expression-based retrospective study. Plos Med. *13*, e1002194. https://doi.org/10.1371/journal.pmed.1002194.

Anders, S., Pyl, P.T., and Huber, W. (2015). HTSeq–a Python framework to work with high-throughput sequencing data. Bioinformatics *31*, 166–169. https://doi.org/10.1093/bioinformatics/btu638.

Ascierto, M.L., Idowu, M.O., Zhao, Y., Khalak, H., Payne, K.K., Wang, X.Y., Dumur, C.I., Bedognetti, D., Tomei, S., Ascierto, P.A., et al. (2013). Molecular signatures mostly associated with NK cells are predictive of relapse free survival in breast cancer patients. J. Transl. Med. *11*, 145. https://doi.org/10.1186/1479-5876-11-145.

Aslakson, C.J., and Miller, F.R. (1992). Selective events in the metastatic process defined by analysis of the sequential dissemination of subpopulations of a mouse mammary tumor. Cancer Res. *52*, 1399–1405.

Baklaushev, V.P., Kilpelainen, A., Petkov, S., Abakumov, M.A., Grinenko, N.F., Yusubalieva, G.M., Latanova, A.A., Gubskiy, I.L., Zabozlaev, F.G., Starodubova, E.S., et al. (2017). Luciferase expression allows bioluminescence imaging but imposes limitations on the orthotopic mouse (4T1) model of breast cancer. Sci. Rep. *7*, 7715. https://doi.org/10.1038/s41598-017-07851-z.

Barnhart, B.C., Legembre, P., Pietras, E., Bubici, C., Franzoso, G., and Peter, M.E. (2004). CD95 ligand induces motility and invasiveness of apoptosis-resistant tumor cells. EMBO J. *23*, 3175–3185.

Baxter, A.G., and Cooke, A. (1993). Complement lytic activity has no role in the pathogenesis of autoimmune diabetes in NOD mice. Diabetes *42*, 1574–1578. https://doi.org/10.2337/diab.42.11.1574.

Blok, E.J., van den Bulk, J., Dekker-Ensink, N.G., Derr, R., Kanters, C., Bastiaannet, E., Kroep, J.R., van de Velde, C.J., and Kuppen, P.J. (2017). Combined evaluation of the FAS cell surface death receptor and CD8+ tumor infiltrating lymphocytes as a prognostic biomarker in breast cancer. Oncotarget *8*, 15610–15620. https://doi.org/10.18632/oncotarget.14779.

Briggs, L.C., Chan, A.W.E., Davis, C.A., Whitelock, N., Hotiana, H.A., Baratchian, M., Bagneris, C., Selwood, D.L., Collins, M.K., and Barrett, T.E. (2017). IKKgamma-mimetic peptides block the resistance to apoptosis associated with Kaposi's sarcoma-associated herpesvirus infection. J. Virol. *91*. https://doi.org/10.1128/JVI.01170-17.

Cai, Z., Yang, F., Yu, L., Yu, Z., Jiang, L., Wang, Q., Yang, Y., Wang, L., Cao, X., and Wang, J. (2012). Activated T cell exosomes promote tumor invasion via Fas signaling pathway. J. Immunol. *188*, 5954–5961. https://doi.org/10.4049/jimmunol.1103466.

Ceppi, P., Hadji, A., Kohlhapp, F., Pattanayak, A., Hau, A., Xia, L., Liu, H., Murmann, A.E., and Peter, M.E. (2014). CD95 and CD95L promote and protect cancer stem cells. Nat. Commun. *5*, 5238.

Chen, L., Park, S.M., Tumanov, A.V., Hau, A., Sawada, K., Feig, C., Turner, J.R., Fu, Y.X., Romero, I.L., Lengyel, E., and Peter, M.E. (2010). CD95 promotes tumour growth. Nature *465*, 492–496.

Christofori, G. (2006). New signals from the invasive front. Nature *441*, 444–450. nature04872 [pii]. https://doi.org/10.1038/nature04872.

DeSantis, C.E., Fedewa, S.A., Goding Sauer, A., Kramer, J.L., Smith, R.A., and Jemal, A. (2016). Breast cancer statistics, 2015: convergence of incidence rates between black and white women. CA A. Cancer J. Clin. *66*, 31–42. https://doi.org/10.3322/caac.21320.

Dobin, A., Davis, C.A., Schlesinger, F., Drenkow, J., Zaleski, C., Jha, S., Batut, P., Chaisson, M., and Gingeras, T.R. (2013). STAR: ultrafast universal RNA-seq aligner. Bioinformatics *29*, 15–21. https://doi.org/10.1093/bioinformatics/bts635.

Drachsler, M., Kleber, S., Mateos, A., Volk, K., Mohr, N., Chen, S., Cirovic, B., Tuttenberg, J., Gieffers, C., Sykora, J., et al. (2016). CD95 maintains stem cell-like and non-classical EMT programs in primary human glioblastoma cells. Cell Death Dis. *7*, e2209. https://doi.org/10.1038/cddis.2016.102.

Feig, C., Tchikov, V., Schutze, S., and Peter, M.E. (2007). Palmitoylation of CD95 facilitates formation of SDS-stable receptor aggregates that initiate apoptosis signaling. EMBO J. *26*, 221–231.

Guegan, J.P., Ginestier, C., Charafe-Jauffret, E., Ducret, T., Quignard, J.F., Vacher, P., and Legembre, P. (2020). CD95/Fas and metastatic disease: what does not kill you makes you stronger. Semin. Cancer Biol. *60*, 121–131. https://doi.org/10.1016/j.semcancer.2019.06.004.

Guegan, J.P., Pollet, J., Ginestier, C., Charafe-Jauffret, E., Peter, M.E., and Legembre, P. (2021). CD95 expression in triple negative breast cancer blocks induction of an inflammatory state through differential regulation of NF-kB Signaling. bioRxiv. [PREPRINT]. https://doi.org/10.1101/2021.04.07.438830.

Gulculer Balta, G.S., Monzel, C., Kleber, S., Beaudouin, J., Balta, E., Kaindl, T., Chen, S., Gao, L., Thiemann, M., Wirtz, C.R., et al. (2019). 3D cellular architecture modulates tyrosine kinase activity, thereby switching CD95-mediated apoptosis to survival. Cell Rep. *29*, 2295–2306 e96. https://doi.org/10.1016/j.celrep.2019.10.054.

Hadji, A., Ceppi, P., Murmann, A.E., Brockway, S., Pattanayak, A., Bhinder, B., Hau, A., De Chant, S., Parimi, V., Kolesza, P., et al. (2014). Death induced by CD95 or CD95 ligand elimination. Cell Rep. *10*, 208–222.

Hoogwater, F.J., Nijkamp, M.W., Smakman, N., Steller, E.J., Emmink, B.L., Westendorp, B.F., Raats, D.A., Sprick, M.R., Schaefer, U., Van Houdt, W.J., et al. (2010). Oncogenic K-Ras turns death receptors into metastasis-promoting receptors in human and mouse colorectal cancer cells. Gastroenterology *138*, 2357–2367. https://doi.org/10.1053/j.gastro.2010.02.046.

Ibrahim, E.M., Al-Foheidi, M.E., Al-Mansour, M.M., and Kazkaz, G.A. (2014). The prognostic value of tumor-infiltrating lymphocytes in triple-negative breast cancer: a meta-analysis. Breast Cancer Res. Treat. *148*, 467–476. https://doi.org/10.1007/s10549-014-3185-2.

Jablonski, K.A., Amici, S.A., Webb, L.M., Ruiz-Rosado Jde, D., Popovich, P.G., Partida-Sanchez, S., and Guerau-de-Arellano, M. (2015). Novel markers to delineate murine M1 and M2 macrophages. PLoS One *10*, e0145342. https://doi.org/10.1371/journal.pone.0145342.

Kleber, S., Sancho-Martinez, I., Wiestler, B., Beisel, A., Gieffers, C., Hill, O., Thiemann, M., Mueller, W., Sykora, J., Kuhn, A., et al. (2008). Yes and PI3K bind CD95 to signal invasion of glioblastoma. Cancer Cell *13*, 235–248.

Krammer, P.H. (2000). CD95's deadly mission in the immune system. Nature *407*, 789–795.

Kravtsova-Ivantsiv, Y., Shomer, I., Cohen-Kaplan, V., Snijder, B., Superti-Furga, G., Gonen, H., Sommer, T., Ziv, T., Admon, A., and Naroditsky, I. (2015). KPC1-mediated ubiquitination and proteasomal processing of NF-κB1 p105 to p50 restricts tumor growth. Cell. *161*, 333–347. https://doi.org/10.1016/j.cell.2015.03.001.

Kreso, A., and Dick, J.E. (2014). Evolution of the cancer stem cell model. Cell Stem Cell *14*, 275–291. https://doi.org/10.1016/j.stem.2014.02.006.

Lelekakis, M., Moseley, J.M., Martin, T.J., Hards, D., Williams, E., Ho, P., Lowen, D., Javni, J., Miller, F.R., Slavin, J., and Anderson, R.L. (1999). A novel orthotopic model of breast cancer metastasis to bone. Clin. Exp. Metastasis *17*, 163–170.

Letellier, E., Kumar, S., Sancho-Martinez, I., Krauth, S., Funke-Kaiser, A., Laudenklos, S., Konecki, K., Klussmann, S., Corsini, N.S., Kleber, S., et al. (2010). CD95-ligand on peripheral myeloid cells activates Syk kinase to trigger their recruitment to the inflammatory site. Immunity *32*, 240–252. S1074-7613(10)00041-5 [pii]. https://doi.org/10.1016/j.immuni.2010.01.011.

Li, H., Fan, X., Stoicov, C., Liu, J.H., Zubair, S., Tsai, E., Ste Marie, R., Wang, T.C., Lyle, S., Kurt-Jones, E., and Houghton, J. (2009). Human and mouse colon cancer utilizes CD95 signaling for local growth and metastatic spread to liver. Gastroenterology *137*, 934–944.

Lin, H.C., Lai, P.Y., Lin, Y.P., Huang, J.Y., and Yang, B.C. (2012). Fas ligand enhances malignant behavior of tumor cells through interaction with Met, hepatocyte growth factor receptor, in lipid rafts. J. Biol. Chem. *287*, 20664–20673. https://doi.org/10.1074/jbc.M111.326058.

Liu, Q., Tan, Q., Zheng, Y., Chen, K., Qian, C., Li, N., Wang, Q., and Cao, X. (2014). Blockade of Fas signaling in breast cancer cells suppresses tumor growth and metastasis via disruption of Fas signaling-initiated cancer-related inflammation. J. Biol. Chem. *289*, 11522–11535. https://doi.org/10.1074/jbc.M113.525014.

Lois, C., Hong, E.J., Pease, S., Brown, E.J., and Baltimore, D. (2002). Germline transmission and tissue-specific expression of transgenes delivered by lentiviral vectors. Science *295*, 868–872. https://doi.org/10.1126/science.1067081.

Love, M.I., Huber, W., and Anders, S. (2014). Moderated estimation of fold change and dispersion for RNA-seq data with DESeq2. Genome Biol. *15*, 550. https://doi.org/10.1186/s13059-014-0550-8.

Malleter, M., Tauzin, S., Bessede, A., Castellano, R., Goubard, A., Godey, F., Leveque, J., Jezequel, P., Campion, L., Campone, M., et al. (2013). CD95L cell surface cleavage triggers a prometastatic signaling pathway in triple-negative breast cancer. Cancer Res. *73*, 6711–6721. https://doi.org/10.1158/0008-5472.CAN-13-1794.

Mapara, M.Y., Bargou, R., Zugck, C., Dohner, H., Ustaoglu, F., Jonker, R.R., Krammer, P.H., and Dorken, B. (1993). APO-1 mediated apoptosis or proliferation in human chronic B lymphocytic leukemia: correlation with bcl-2 oncogene expression. Eur. J. Immunol. *23*, 702–708.

Martin, M. (2011). Cutadapt removes adapter sequences from high-throughput sequencing reads. EMBnet.journal *7*, 10–12.

Martin-Villalba, A., Llorens-Bobadilla, E., and Wollny, D. (2013). CD95 in cancer: tool or target? Trends Mol. Med. *19*, 329–335.

Marvel, D., and Gabrilovich, D.I. (2015). Myeloid-derived suppressor cells in the tumor microenvironment: expect the unexpected. J. Clin. Invest. *125*, 3356–3364. https://doi.org/10.1172/JCI80005.

Miller, F.R., Miller, B.E., and Heppner, G.H. (1983). Characterization of metastatic heterogeneity among subpopulations of a single mouse mammary tumor: heterogeneity in phenotypic stability. Invasion Metastasis *3*, 22–31.

Nagata, S. (1999). Fas ligand-induced apoptosis. Annu. Rev. Genet. *33*, 29–55.

Ouzounova, M., Lee, E., Piranlioglu, R., El Andaloussi, A., Kolhe, R., Demirci, M.F., Marasco, D., Asm, I., Chadli, A., Hassan, K.A., et al. (2017). Monocytic and granulocytic myeloid derived suppressor cells differentially regulate spatiotemporal tumour plasticity during metastatic cascade. Nat. Commun. *8*, 14979. https://doi.org/10.1038/ncomms14979.

Parrish-Novak, J., Dillon, S.R., Nelson, A., Hammond, A., Sprecher, C., Gross, J.A., Johnston, J., Madden, K., Xu, W., West, J., et al. (2000). Interleukin 21 and its receptor are involved in NK cell expansion and regulation of lymphocyte function. Nature *408*, 57–63. https://doi.org/10.1038/35040504.

Peranzoni, E., Zilio, S., Marigo, I., Dolcetti, L., Zanovello, P., Mandruzzato, S., and Bronte, V. (2010). Myeloid-derived suppressor cell heterogeneity and subset definition. Curr. Opin. Immunol. *22*, 238–244. https://doi.org/10.1016/j.coi.2010.01.021.

Peter, M.E., Barnhart, B.C., and Algeciras-Schimnich, A. (2003). CD95L/FasL and its Receptor CD95 (APO-1/Fas), 4th Edition (Academic Press).

Peter, M.E., Budd, R.C., Desbarats, J., Hedrick, S.M., Hueber, A.O., Newell, M.K., Owen, L.B., Pope, R.M., Tschopp, J., Wajant, H., et al. (2007). The CD95 receptor: apoptosis revisited. Cell *129*, 447–450.

Peter, M.E., Hadji, A., Murmann, A.E., Brockway, S., Putzbach, W., Pattanayak, A., and Ceppi, P. (2015). The role of CD95 and CD95 ligand in cancer. Cell Death Differ. *22*, 885–886. https://doi.org/10.1038/cdd.2015.25.

Picelli, S., Faridani, O.R., Bjorklund, A.K., Winberg, G., Sagasser, S., and Sandberg, R. (2014). Full-length RNA-seq from single cells using Smart-seq2. Nat. Protoc. *9*, 171–181. https://doi.org/10.1038/nprot.2014.006.

Presa, M., Chen, Y.G., Grier, A.E., Leiter, E.H., Brehm, M.A., Greiner, D.L., Shultz, L.D., and Serreze, D.V. (2015). The presence and preferential activation of regulatory T cells diminish adoptive transfer of autoimmune diabetes by polyclonal nonobese diabetic (NOD) T cell effectors into NSG versus NOD-scid mice. J. Immunol. *195*, 3011–3019. https://doi.org/10.4049/jimmunol.1402446.

Priceman, S.J., Sung, J.L., Shaposhnik, Z., Burton, J.B., Torres-Collado, A.X., Moughon, D.L., Johnson, M., Lusis, A.J., Cohen, D.A., Iruela-Arispe, M.L., and Wu, L. (2010). Targeting distinct tumor-infiltrating myeloid cells by inhibiting CSF-1 receptor: combating tumor evasion of antiangiogenic therapy. Blood *115*, 1461–1471. https://doi.org/10.1182/blood-2009-08-237412.

Putzbach, W., Gao, Q.Q., Patel, M., van Dongen, S., Haluck-Kangas, A., Sarshad, A.A., Bartom, E., Kim, K.Y., Scholtens, D.M., Hafner, M., et al. (2017). Many si/shRNAs can kill cancer cells by targeting multiple survival genes through an off-target mechanism. eLife *6*, e29702.

Putzbach, W., Haluck-Kangas, A., Gao, Q.Q., Sarshad, A.A., Bartom, E.T., Stults, A., Qadir, A.S., Hafner, M., and Peter, M.E. (2018). CD95/Fas ligand mRNA is toxic to cells. eLife *7*, e38621.

Qadir, A.S., Ceppi, P., Brockway, S., Law, C., Mu, L., Khodarev, N.N., Kim, J., Zhao, J.C., Putzbach, W., Murmann, A.E., et al. (2017). CD95/Fas increases stemness in cancer cells by inducing a STAT1-dependent type I interferon response. Cell Rep. *18*, 2373–2386. https://doi.org/10.1016/j.celrep.2017.02.037.

Qadir, A.S., Stults, A.M., Murmann, A.E., and Peter, M.E. (2020). The mechanism of how CD95/Fas activates the Type I IFN/STAT1 axis, driving cancer stemness in breast cancer. Sci. Rep. *10*, 1310. https://doi.org/10.1038/s41598-020-58211-3.

Ries, C.H., Cannarile, M.A., Hoves, S., Benz, J., Wartha, K., Runza, V., Rey-Giraud, F., Pradel, L.P., Feuerhake, F., Klaman, I., et al. (2014). Targeting tumor-associated macrophages with anti-CSF-1R antibody reveals a strategy for cancer therapy. Cancer Cell *25*, 846–859. https://doi.org/10.1016/j.ccr.2014.05.016.

Serreze, D.V. (1993). Autoimmune diabetes results from genetic defects manifest by antigen presenting cells. Faseb. J. *7*, 1092–1096. https://doi.org/10.1096/fasebj.7.11.8370480.

Shultz, L.D., Ishikawa, F., and Greiner, D.L. (2007). Humanized mice in translational biomedical research. Nat. Rev. Immunol. *7*, 118–130. https://doi.org/10.1038/nri2017.

Shultz, L.D., Brehm, M.A., Garcia-Martinez, J.V., and Greiner, D.L. (2012). Humanized mice for immune system investigation: progress, promise and challenges. Nat. Rev. Immunol. *12*, 786–798. https://doi.org/10.1038/nri3311.

Sinha, P., Chornoguz, O., Clements, V.K., Artemenko, K.A., Zubarev, R.A., and Ostrand-Rosenberg, S. (2011). Myeloid-derived suppressor cells express the death receptor Fas and apoptose in response to T cell-expressed FasL. Blood *117*, 5381–5390. https://doi.org/10.1182/blood-2010-11-321752.

Strasser, A., Jost, P.J., and Nagata, S. (2009). The many roles of FAS receptor signaling in the immune system. Immunity *30*, 180–192.

Swierczak, A., Cook, A.D., Lenzo, J.C., Restall, C.M., Doherty, J.P., Anderson, R.L., and Hamilton, J.A. (2014). The promotion of breast cancer metastasis caused by inhibition of CSF-1R/CSF-1 signaling is blocked by targeting the G-CSF receptor. Cancer Immunol. Res. *2*, 765–776. https://doi.org/10.1158/2326-6066.CIR-13-0190.

Takaki, R., Hayakawa, Y., Nelson, A., Sivakumar, P.V., Hughes, S., Smyth, M.J., and Lanier, L.L. (2005). IL-21 enhances tumor rejection through a NKG2D-dependent mechanism. J. Immunol. *175*, 2167–2173. https://doi.org/10.4049/jimmunol.175.4.2167.

Teodorczyk, M., Kleber, S., Wollny, D., Sefrin, J.P., Aykut, B., Mateos, A., Herhaus, P., Sancho-Martinez, I., Hill, O., Gieffers, C., et al. (2015). CD95 promotes metastatic spread via Sck in pancreatic ductal adenocarcinoma. Cell Death Differ. *22*, 1192–1202. https://doi.org/10.1038/cdd.2014.217.

Trauzold, A., Roder, C., Sipos, B., Karsten, K., Arlt, A., Jiang, P., Martin-Subero, J.I., Siegmund, D., Muerkoster, S., Pagerols-Raluy, L., et al. (2005). CD95 and TRAF2 promote invasiveness of pancreatic cancer cells. Faseb. J. *19*, 620–622.

Ugel, S., De Sanctis, F., Mandruzzato, S., and Bronte, V. (2015). Tumor-induced myeloid deviation: when myeloid-derived suppressor cells meet tumor-associated macrophages. J. Clin. Invest. *125*, 3365–3376. https://doi.org/10.1172/JCI80006.

Wajant, H., Pfizenmaier, K., and Scheurich, P. (2003). Non-apoptotic Fas signaling. Cytokine Growth Factor Rev. *14*, 53–66.

Walczak, H., Miller, R.E., Ariail, K., Gliniak, B., Griffith, T.S., Kubin, M., Chin, W., Jones, J., Woodward, A., Le, T., et al. (1999). Tumoricidal activity of tumor necrosis factor-related apoptosis-inducing ligand in vivo. Nat. Med. *5*, 157–163.

Wick, W., Fricke, H., Junge, K., Kobyakov, G., Martens, T., Heese, O., Wiestler, B., Schliesser, M.G., von Deimling, A., Pichler, J., et al. (2014). A phase II, randomized, study of weekly APG101+reirradiation versus reirradiation in progressive glioblastoma. Clin. Cancer Res. *20*, 6304–6313. https://doi.org/10.1158/1078-0432.CCR-14-0951-T.

Wick, W., Dettmer, S., Berberich, A., Kessler, T., Karapanagiotou-Schenkel, I., Wick, A., Winkler, F., Pfaff, E., Brors, B., Debus, J., et al. (2019a). N2M2 (NOA-20) phase I/II trial of molecularly matched targeted therapies plus radiotherapy in patients with newly diagnosed non-MGMT hypermethylated glioblastoma. Neuro Oncol. *21*, 95–105. https://doi.org/10.1093/neuonc/noy161.

Wick, W., Krendyukov, A., Junge, K., Hoger, T., and Fricke, H. (2019b). Longitudinal analysis of quality of life following treatment with Asunercept plus reirradiation versus reirradiation in progressive glioblastoma patients. J. Neurooncol. *145*, 531–540. https://doi.org/10.1007/s11060-019-03320-x.

Youn, J.I., Nagaraj, S., Collazo, M., and Gabrilovich, D.I. (2008). Subsets of myeloid-derived suppressor cells in tumor-bearing mice. J. Immunol. *181*, 5791–5802. https://doi.org/10.4049/jimmunol.181.8.5791.

Zheng, H.X., Cai, Y.D., Wang, Y.D., Cui, X.B., Xie, T.T., Li, W.J., Peng, L., Zhang, Y., Wang, Z.Q., Wang, J., and Jiang, B. (2013). Fas signaling promotes motility and metastasis through epithelial-mesenchymal transition in gastrointestinal cancer. Oncogene *32*, 1183–1192.

STAR★METHODS

KEY RESOURCES TABLE

REAGENT or RESOURCE	SOURCE	IDENTIFIER
Antibodies		
Phospho-Stat1 (Tyr701) (58D6) Rabbit mAb	Cell Signaling Technologies	Cat.# 9167; RRID: AB_561284
PECAM-1 Antibody (M-20)-CD31	Santa Cruz	Cat.# sc-1506; RRID: AB_216103
Rat anti-Mouse Ly-6G	BD Bioscience	Cat.# 551459; RRID: AB_394206
Recombinant Anti-CD11b antibody [EPR1344]	Abcam	Cat.# ab133357; RRID: AB_2650514
FOXP3 Monoclonal Antibody (FJK-16s)	eBioscience™	Cat.# 14-5773-82; RRID: AB_467576
Mouse NKp46/NCR1 Antibody	R&D Systems	Cat.# AF2225; RRID: AB_355192
CD8a Monoclonal Antibody (4SM16)	eBioscience™	Cat.# 14-0195-82; RRID: AB_2637159
CD4 Monoclonal Antibody (4SM95)	eBioscience™	Cat.# 14-9766-82; RRID: AB_2573008
F4/80 Monoclonal Antibody (BM8)	eBioscience™	Cat.# 14-4801; RRID: AB_467558
Biotin-SP-AffiniPure donkey anti-rabbit IgG (H+L)	Jackson ImmunoResearch Laboratories	Cat.# 711-065-152; RRID: AB_2340593
Biotin-SP-AffiniPure donkey anti-rat IgG (H+L)	Jackson ImmunoResearch Laboratories	Cat.# 712-065-153; RRID: AB_2315779
PE conjugated-anti-CD95	eBioscience™	Cat.# 12-0951-83; RRID: AB_465789
PE conjugated Isotype control	eBioscience™	Cat.# 12-4714-82; RRID: AB_470060
Isotype Rat IgG2b control	eBioscience™	Cat.# 17-4031-82; RRID: AB_470176
anti-CD44-APC conjugated	eBioscience™	Cat.# 17-0441-82; RRID: AB_469390
CCR4-BV421	Biolegend	Cat.# 131218; RRID: AB_2650890
CXCR5-BV605	Biolegend	Cat.# 145513; RRID: AB_2562208
CD8-BV650	Biolegend	Cat.# 100742; RRID: AB_2564509
CXCR3-BV711	BD Bioscience	Cat.# 740825; RRID: AB_2740483
CD45-BV785	Biolegend	Cat.# 103149; RRID: AB_2564590
CCR6-PE/Dazzle594	Biolegend	Cat.# 129822; RRID: AB_2687019
F4/80-BV605	Biolegend	Cat.# 123133; RRID: AB_2562305
Gr1-PE/Dazzle594	Biolegend	Cat.# 108452; RRID: AB_2564249
Ly6C-PE/Cy7	Biolegend	Cat.# 128017; RRID: AB_1732093
Ly6G-APC	Biolegend	Cat.# 127613; RRID: AB_1877163
CD11b-BV510	Biolegend	Cat.# 101263; RRID: AB_2629529
FoxP3-BV421	Biolegend	Cat.# 126419; RRID: AB_2565933
CD4-AF488	Biolegend	Cat.# 100532; RRID: AB_493373
CD3-PerCP/Cy5.5	Biolegend	Cat.# 100218; RRID: AB_1595492
CD38-PE-Dazzle594	Biolegend	Cat.# 102729; RRID: AB_2632890
CD25-PE/Cy7	Biolegend	Cat.# 102015; RRID: AB_312865
anti-mouse CD8 mAb (clone 53-6.7)	BioXCell	Cat.# BE0004-1; RRID: AB_1107671
IgG2a isotype control (clone 2A3)	BioXCell	Cat.# BE0089; RRID: AB_1107769
anti-mouse CD4 mAb (clone GK1.5)	BioXCell	Cat.# BE0003-1; RRID: AB_1107636
IgG2b isotype control (clone 2.43)	BioXCell	Cat.# BP0090; RRID: AB_2891360
anti-Asialo GM1 rabbit polyclonal antibody	Thermo Fisher Scientific	Cat.# 16-6507-39; RRID: AB_10718540
Polyclonal rabbit IgG	Thermo Fisher Scientific	Cat.# 31235; RRID: AB_243593
anti-mouse CSF1-R mAb (clone AFS98)	BioXCell	Cat.# BP0213; RRID: AB_2894813
Bacterial and virus strains		
pFU-L2G luciferase lentivirus	Dr. Sanjiv Sam Gambhir at Stanford University, Stanford CA	Lois et al., 2002

(*Continued on next page*)

Continued

REAGENT or RESOURCE	SOURCE	IDENTIFIER
Biological samples		
lentiCas9-Blast virus	Addgene	Cat.# 52962
PX459-V2 plasmid	Addgene	Cat.# 62988
Zombie NIR	Biolegend	Cat.# 423106
Chemicals, peptides, and recombinant proteins		
RPMI 1640 medium	Fisher Scientific	Cat.# 10040CM
Fetal bovine serum (FBS)	Sigma-Aldrich	Cat.# 14009C
L-glutamine	Fisher Scientific	Cat.# 25-005CI
Penicillin/Streptomycin	Fisher Scientific	Cat.# 30-002-CI
IFNβ	pbl Assay Science	Cat.# 11415-1
Leucine zipper tagged CD95L (LzCD95L)	Henning Walzcak (University College of London Cancer Institute)	(Walczak et al., 1999)
Propidium iodide	Sigma-Aldrich	Cat.# P4864
Bovine serum albumin	Sigma-Aldrich	Cat.# A7906
Puromycin	Sigma-Aldrich	Cat.# P9620
Blasticidin	InvivoGen	Cat.# ant-bl-1
G418	Sigma-Aldrich	Cat.# G8168
Hydrocortisone	Sigma-Aldrich	Cat.# H0888
Polybrene	Sigma-Aldrich	Cat.# H9268
TransIT-X2 transfecting reagent	Mirus	Cat.# MIR 6003
Lipofectamine 3000	Thermo Fisher Scientific	Cat.# L3000015
Epicult media	Stem Cell Technology	Cat.# 5630
Mammocult media	Stem Cell Technology	Cat.# 5620
Heparin	Stem Cell Technology	Cat.# 07980
Trypan blue solution	Lonza	Cat.# 17-942-E
Matrigel	Trevigen	Cat.# 3432-010-01
Normal buffered formalin	VWR	Cat.# 16004-128
DNAse Set	Qiagen	Cat.# 79254
Critical commercial assays		
EdU flow cytometry kit 488 EdU	Sigma-Aldrich	Cat.# BCK-FC488-50
Aldefluor kit	Stem Cell Technologies	Cat.# 1700
Tumor Dissociation Kit, mouse	Miltenyi Biotec	Cat.# 130-096-730
QIAzol lysis reagent	Qiagen	Cat.# 79306
High-Capacity cDNA Reverse Transcription Kit	Applied Biosystems	Cat.# 4368814
miRNeasy Mini Kit	Qiagen Sciences	Cat.# 217004
KAPA HiFi HotStart master mix (KK2601)	Roche Sequencing Store	Cat.# KK2601
TRIzol	Invitrogen	Cat.# 15596018
Deposited data		
RNAseq data of the 4T1 wt and CD95 k.o cell lines	Peter Lab	GEO: GSE154676
RNAseq data of 4T1 wt and CD95 k.o tumors grown in NGS and Balb/c mice	Peter Lab	GEO: GSE154682
Experimental models: Cell lines		
4T1 cell line to generate the F- and U-clones	American Type Culture Collection (ATCC)	Cat# CRL-2539

(*Continued on next page*)

Continued

REAGENT or RESOURCE	SOURCE	IDENTIFIER
Experimental models: Organisms/strains		
NOD.Cg-Prkdc^{scid} Il2rg^{tm1Wjl}/SzJ (NSG) mice	Jackson laboratory	Stock #: 005557
Balb/cJ mice	Jackson laboratory	Stock #: 000651
NOD/Shi-scid/IL-2Rnull (NSG) mice	Charles River, France	Strain code: 614
NOD.CB17-Prkdc^{scid}/NCrCrl (NOD/SCID) mice	Charles River, France	Strain code: 394
Balb/cByJ mice	Charles River, France	Strain code: 028
Oligonucleotides		
mGAPDH	Life technologies	Mm99999915_g1
Exon9 specific mCD95	Life technologies	Mm01204974_m1
Exon 1-2 specific mCD95	Life technologies	Mm00433237_m1
mCD95L	Life technologies	Mm00438864_m1
mSTAT1	Life technologies	Mm01257286_m1
mPLSCR1	Life technologies	Mm01228223_g1
mBMI1	Life technologies	Mm03053308_g1
mZEB1	Life technologies	Mm00495564_m1
mZEB2	Life technologies	Mm00497196_m1
Software and algorithms		
FlowJo version 8.8.6 (Treestar Inc).	Becton, Dickinson & Company	https://www.flowjo.com/
Novoexpress software	Agilent	https://www.agilent.com/en/product/research-flow-cytometry/flow-cytometry-software/novocyte-novoexpress-software-1320805
NDP (NanoZoomer Digital Pathology)	Hamamatsu Inc	https://www.hamamatsu.com/us/en/product/type/U12388-01/index.html)
Visiopharm Image analysis Suite	VIS, Horsholm, Denmark	https://visiopharm.com
Prism Software	Graphpad Software	https://www.graphpad.com/
Other		
IncuCyte Zoom	Essen Bioscience	Cat.#: FLR30140
IncuCute Zoom sofware version 2016A	Essen Bioscience	Essenbioscience.com
Novocyte Quanteon cytometer	Agilent	Cat.#: 2010097

RESOURCE AVAILABILITY

Lead contact

Further information and requests for resources should be directed to and will be fulfilled by the lead contact Marcus Peter, E-mail: m-peter@northwestern.edu.

Materials availability

Materials generated in this study can be made available upon request to the Lead Contact.

Data and code availability

Data availability. Sequencing data have been deposited in the National Cancer for Biotechnology Information Gene Expression Omnibus with accession number GSE154676 (https://www.ncbi.nlm.nih.gov/geo/query/acc.cgi?acc=GSE154676, for the RNAseq analysis of the cell lines) and GSE154682 (https://www.ncbi.nlm.nih.gov/geo/query/acc.cgi?acc=GSE154682, for the RNAseq data of the tumors grown in mice).

This paper does not report original code.

Any additional information required to reanalyze the data reported in this paper is available from the lead contact upon request.

EXPERIMENTAL MODEL AND SUBJECT DETAILS

Cell lines

The mouse breast cancer cell line to generate the U-clones 4T1 was purchased from the ATCC and cultured in RPMI 1640 medium (Mediatech Inc) containing 10% heat-inactivated fetal bovine serum (FBS) (Sigma-Aldrich), 1% L-glutamine (Mediatech Inc) and 1% penicillin/streptomycin (Mediatech Inc). The 4T1 cell line to generate the F-clones was purchased from ATCC (Molsheim Cedex, France) and cultured in RPMI supplemented with 8% heat-inactivated FCS (v/v) and 2 mM L-glutamine at 37°C/5% CO_2.

Animal studies

Animal studies in the US were performed according to the Northwestern University Institutional Animal Care and Use Committee (IACUC)-approved protocol. Animal studies in France were conducted under EU and French animal welfare regulations for animal use in experimentation (European Directive 2010/63/EU and French decree and orders of February 1st, 2013) and approved by local ethics committee (Agreement no. #16487-2018082108541206 v3).

Growth of 4T1 cells in NGS and Balb/c mice

U-clones: 4T1 vCas9 (wt) and CD95 k.o. clones #54 and #69 were infected with pFU-L2G luciferase lentivirus as previously described (Ceppi et al., 2014). Then cells (1×10^5) of wt or a 1:1 mixture of the CD95 k.o. clones were injected in 100 µl PBS and Matrigel (Cat#3432-010-01, Trevigen) (1:1 ratio) into the fourth mammary fat pad at the base of the nipple into female NOD-scid-gamma (NSG) mice and Balb/c mice (Jackson lab). Growth of tumors was monitored weekly by using an IVIS Spectrum *in vivo* imaging system and luminescence was quantified at the regions of interest (ROI = the same area for each mouse encompassing the entire mammary gland) using the Living Image software. For some experiments L2G luciferase (Luc-neo) infected cells were further infected with NucLight Red Lentivirus Reagent (EF-1 alpha promoter, Puromycin selection, Essen Bioscience) and the stable cells were individually injected into the fourth mammary. In some cases unmodified cells were injected. In other experiments 4T1 CD95 k.o. #54 cells (1×10^5) (Luc-neo/Nuc-red) and CD95 k.o. #69 cells (Luc-neo/Nuc-red) were injected into same mouse. To grow F-clones *in vivo*: $5x10^4$ cells in PBS were injected in the fourth mammary fat pad at the base of the nipple into female Balb/c (Charles River, France). From Day 6, tumor volume was measured with a set of calipers and calculated by using the following formula: volume = (length×width2)/2. A colony of immunocompromised NSG mice (NOD/SCID/IL2rγnull) was maintained in house under aseptic sterile conditions. After two weeks of injection, tumor volume was measured with a set of calipers and calculated by using the following formula: volume = (length×$width^2$)/2.

METHOD DETAILS

Reagents

Leucine zipper tagged CD95L (LzCD95L) was used to induce apoptosis at 100 ng/ml as described before unless otherwise specified (Qadir et al., 2017). IFNβ (11415-1) (used at 1000U/ml) was purchased from pbl Assay Science. Propidium iodide (#P4864), bovine serum albumin (BSA), EdU flow cytometry kit 488, puromycin, G418 and hydrocortisone were purchased from Sigma-Aldrich. Blasticidin was purchased from InvivoGen. Reagents used for flow cytometry, anti-CD44-APC conjugated (17-0441-82), Isotype Rat IgG2b control (17-4031-82), PE conjugated-anti-CD95 (2-0951-83) and PE conjugated Isotype control (12-4714-82) were from eBioscience. The Aldefluor kit (Stem Cell Technologies) was used for the staining and quantification of ALDH1 activity by flow cytometry. Gates were based on the analysis of cells treated with the specific inhibiting reagent DEAB as a negative control following the instructions by the manufacturer. For the immune histochemistry (IHC) of tumor slides samples the following primary antibodies were used F4/80 (eBioscience™ # 14-4801), CD4 (eBioscience™ #14-9766-82), CD8 (eBioscience™ #14-0195-82), pSTAT1 (Cell Signaling #9167), CD31 (Santa Cruz #sc-1506), Ly6G (BD Bioscience #551459), CD11b (Abcam #ab133357), FOXP3 (eBioscience™ #14-5773-82), and NKp46 (R&D Systems, AF2225). The secondary antibodies Biotin-SP-AffiniPure donkey anti-rabbit IgG (H+L) (#711-065-152) and Biotin-SP-AffiniPure donkey anti-rat IgG (H+L) (#712-065-153) were from Jackson ImmunoResearch Laboratories.

CRISPR/Cas9 mediated deletion of CD95

Generation of the CD95 k.o. U-clones: In order to generate CD95 k.o. 4T1 clones, first stably expressing lentiCas9-Blast-4T1 cell (vCas9-4T1) lines were established. The lentiCas9-Blast virus was obtained from the viral core facility of Northwestern University. 4T1 cells (10^5/well) were plated in 6 well plates and on

the next day cells were infected with the indicated lentiCas9-Blast virus supernatants with polybrene (final concentration: 8 μg/ml). Culture supernatants were replaced with fresh medium containing antibiotics 48 hours after transduction. Uninfected cells were eliminated by a selection medium RPM1-1640 including 4 μg/ml Blasticidin. The two guide RNAs for exon 9 deletion of CD95 gene GCCGGGTTCACATCTGCGC TAGG and CTTGAGGAATCTGATGACCGTGG were designed using the CRISPR design tool available at crispr.mit.edu. The 19-20nt crisprRNA (crRNA) complementary to the target of interest and 67nt transactivating crRNA (tracrRNA), which served as a bridge between the cas9 protein and the crRNA, were ordered from IDT. vCas9-4T1 cells were transfected with crRNA and tracrRNA according the manufactures protocol using TransIT-X2 transfecting reagent (Mirus) in 12 well plates. 3 days after transfection cells were subjected to cell sorting at 1 cell per well directly into 96-well plates. After two to three weeks, single cell clones were expanded and subjected to genotyping and single cell cloning. Deletions in clones were verified by genomic PCR using external and internal primers pairs. To detect the Exon 9 specific deletion in the CD95 gene, external primers were 5′-GGAACAGACCAAGCTTCCGA-3′ (For. primer) and 5′-TCCAGAA CACAGCCATGGTT-3′ (Rev. primer), and two internal reverse primers were 5′-TTGAGTAAATACATCCC GAGAATTG-3′ (For. primer) and 5′-AGCAAGACAACAGAGCAATAGAAAT-3′(Rev. primer) (product size 790bp) and 5′-ATGCATGACAGCATCCAAGA-3′ (For. primer) and 5′-TGCTGGCAAAGAGAACACAC-3′(Rev primer) (product size 338bp). After screening clones, Sanger sequencing was performed to confirm the proper deletion had occurred.

Generation of the CD95 k.o. F-clones: The following sgRNA sequences were cloned within PX459-V2 plasmid and then transfected with lipofectamine 3000 in 4T1 to generate cell lines deficient for CD95 according to manufacturer's instructions. sgRNA sequences target mouse CD95: 5′CACCGCTGCAGAC ATGCTGTGGATC3′ (Fwd), 5′AAACGATCCACAGCATGTCTGCAGC3′ (Rev). After transfection and puromycin selection for 48h, genome-edited cells were cloned by limited dilution and CD95-deficient cells were selected by flow cytometry.

FACS analysis

For CD95 surface-staining cell pellets of about 10^5 cells were resuspended in 100 ml of PBS on ice. After resuspension, 5 μl of either anti-CD95 PE conjugated primary antibody or matching isotype control were added. Cells were incubated on ice at 4°C, in the dark, for 30 min, washed twice with PBS, and percent CD95 positive cells were determined by Becton Dickinson LSR Fortessa at the Flow Cytometry Core Facility of the Northwestern University. ALDH1 activity was quantified as previously described (Ceppi et al., 2014). For CD44 staining, cells were washed twice with PBS and stained with primary antibody or isotype control for 30 min at 4°C in the dark, washed twice with PBS and CD44-APC positive cells were quantified. For the analysis if *ex vivo* tumor, wt and CD95 k.o. 4T1 tumors were extracted and minced with sterile razor blades and incubated for 2 h in the presence of Collagenase (1,000 units per sample) in sterile Epicult media (Stem Cell Technology). Cells were washed with sterile filtered PBS supplemented with 1% bovine serum albumin (PBS-BSA 1%) and filtered through a 40 μm nylon mesh (BD Biosciences). For the detection of ALDH1 or CD44, cells were stained as describe above. Data were analyzed using FlowJo version 8.8.6 (Treestar Inc).

To analyze immune cells infiltrating F-clone in Balb/c mice, tumors were harvested, dissociated on gentleMACS using the tumor dissociation kit (Miltenyi Biotec) and cells (250,000 cells) were stained with the following antibody panels. T lymphocytes-infiltrating tumors were identified using an antibody panel consisting of CCR4-BV421, CXCR5-BV605, CD8-BV650, CXCR3-BV711, CD45-BV785, CD4-AF488, CD3-PerCP/Cy5.5, CCR6-PE/Dazzle594 antibodies and Zombie NIR for cell viability. MDSC and macrophage-infiltrating tumors were stained using CD11b-BV510, F4/80-BV605, CD45-BV785, Gr1-PE/Dazzle594, Ly6C-PE/Cy7, Ly6G-APC antibodies and Zombie NIR for cell viability. M1/M2 cells and Treg cells were monitored in permeabilized cells using FoxP3-BV421, CD11b-BV510, F4/80-BV605, CD45-BV785, CD4-AF488, CD3-PerCP/Cy5.5, CD38-PE-Dazzle594, CD25-PE/Cy7, and Zombie NIR for cell viability. All antibodies used for tumor-infiltrating immune cells came from Biolegend (San Diego, CA, USA). Data were acquired using a Novocyte cytometer (ACEA Biosciences) and analyzed using Novoexpress software.

Sphere forming assays

The single cell sphere formation assay was performed as previously described (Qadir et al., 2017), In brief, cells were pre-treated with LzCD95L, IFNβ, or received no treatment for 6 days. Cell suspensions were passed through a 40 μm sterile cell strainer (Fisher Scientific) to obtain single cells. The strained cell

suspension was serially diluted in Mammocult media (Stem Cell Technology) and seeded at 1 cell/well in ultra-low adherence round bottom 96-well plates (Corning) in triplicate. The cells were cultured in Mammocult media supplemented with 4 μg/ml Heparin (Stem Cell Technology), 0.5 μg/ml hydrocortisone and 10% Mammocult Proliferation Supplement (Stem Cell Technology). After 6-7 days, cultures of U-clones were scanned using IncuCyte Zoom and spheres were counted. For F-clones, spheroids were counted manually. To assess the differences between parental and CD95 k.o. 4T1 cells, the cells were seeded without any treatment.

Cell growth/Proliferation assay

To monitor cell proliferation in parental, vCas9, CD95 k.o. #54 and CD95 k.o. #69 4T1 cells (U-clones), cells were seeded at 1000 cells/well in 96 well plates. Cell growth was monitored in quadruplicate samples at various time points in an IncuCyte Zoom using a confluency mask. To monitor proliferation of 4T1 parental cells with LzCD95L or IFNβ, 1000 cells/well were plated in 96 well, with media containing LzCD95L or IFNβ or no treatment and cell growth was monitored over time.

For F-clones, EdU (5-ethynyl-2'-deoxyuridine) proliferation assay (Sigma-Aldrich) was carried out according to the manufacturer's instructions. Briefly, 4T1 cells were incubated for 1h with 10 μM of the thymidine analog EdU, then washed and fixed with PFA (4%) for 15 min. DNA synthesis (S phase) is associated with EdU incorporation. Finally, iFluor-488, is added and a 'click' chemistry reaction allows its covalent cross-linking to the EdU. Cell proliferation (EdU positive cells) was quantified using the Novocyte flow cytometer.

Cell death assays and cell cycle analysis

To quantify cell death, 50,000 cells were plated in 12 well plates in triplicate and then either left untreated or treated with different concentration of LzCD95L for 24 hr. The total cell pellet consisting of live and dead cells was either re-suspended in lysis buffer (0.1% sodium citrate, pH 7.4, 0.05% Triton X-100, 50 μg/ml propidium iodide), and after incubating for 2-4 hours in the dark at 4°C, percent cell death was quantified by flow cytometry or cells were re-suspended in media and an equal volume of Trypan blue solution (Lonza) was added. Both living and dead (blue) cells were counted on a hemocytometer under a light microscope. To perform cell cycle analysis, 600,000 cells were plated in 6 well plates in triplicate. After 16-20 hours (at ~80% confluence), plates were gently rinsed with PBS and trypsinized to obtain cell pellets. Cell pellets were then washed (resuspended in 2.5 ml PBS, centrifuged at 500 x g for 5 minutes, and then decanted) and resuspended in 500 μl lysis buffer (see above) and kept on ice and protected from light. Immediately before FACS analysis, samples were spiked with 1:500 DAPI solution as a counterstain to assess cell viability (with corresponding no DAPI controls). Samples were then analyzed on a BD FacsAria SORP 6-Laser Cell sorter at the RHLCCC Flow Cytometry Core Facility. Subsequent data were analyzed using FlowJo 10 software.

Real-time PCR

Real-time PCR was performed as described recently (Qadir et al., 2017). In brief, total RNA was extracted using QIAzol Lysis reagent (Qiagen Sciences) and RNA concentration was measured using a NanoDrop 2000. 1-2 μg of total RNA was used to generate cDNA using the High-Capacity cDNA Reverse Transcription Kit (Applied Biosystems). Gene expression in mouse cells was quantified using specific primers from Life technologies for mGAPDH (Mm99999915_g1), Exon9 specific mCD95 (Mm01204974_m1), Exon 1-2 specific mCD95 (Mm00433237_m1), mCD95L (Mm00438864_m1) mSTAT1 (Mm01257286_m1), mPLSCR1 (Mm01228223_g1), mBMI1, (Mm03053308_g1), mZEB1 (Mm00495564_m1) and mZEB2 (Mm00497196_m1) using of the comparative ΔΔCT method and expressed as fold differences.

Depletion of immune cells in mice

To deplete CD8 T cells mice (5 mice/group) were injected i.p. with 200 μg of either anti-mouse CD8 mAb (clone 53-6.7, BioXCell) or IgG2a isotype control (2A3, BioXCell) both in 100 μl. To deplete CD4 T cells mice (5 mice/group) were injected i.p. with 200 μg of either anti-mouse CD4 mAb (GK1.5, BioXCell) or IgG2b isotype control (2.43, BioXCell) both in 100 μl. To deplete NK cells mice (5 mice/group) were injected i.p. with 50 μg of either anti-Asialo GM1 rabbit polyclonal antibody (ThermoFisher) or polyclonal rabbit IgG (ThermoFisher) both in 100 μl. To inhibit CSF1-R mice (5 mice/group) were injected i.p. with 20 mg/kg of either anti-mouse CSF1-R mAb (clone AFS98, BioXCell) or control rat IgG2a (BioXCell) both in 100 μl. Injection frequencies are shown in Figures 3A, 4C, S4A, and S4D.

Immunohistochemistry analysis

Tumors were fixed in 10% normal buffered formalin (VWR, Cat.No.: 16004-128) for 24 hrs, and further processed by the Northwestern University Mouse Histology & Phenotyping Laboratory (MHPL) (paraffin embedding, sectioning at 4 μm, slide preparation, and staining). Tissue sections of each specimen were stained using hematoxylin and Eosin (H&E) staining. The expression of F4/80, CD4, CD8, pSTAT1, CD31, FOXP3, Ly6G, CD11b, and NKp46 was determined in tumor and/or spleen slides. Paraffin sections were dewaxed and blocked with 5% BSA. The sections were then incubated with the relevant antibodies at 4°C overnight. The sections were washed with PBS. For immunohistochemical analysis, sections were incubated with donkey anti-rabbit or donkey anti-rat antibody. Slides were examined and representative fields were photographed at 5x or 20x magnification using a Leica DM4000 B microscope. The immune-positive cells and staining intensities were quantified in a circle that was placed in each staining at the same position in a tumor of the 5x images. For each tumor and condition 8 fields were counted.

IHC quantification

Stained slides on standard size (26 mm x 76 mm) were scanned using NanoZoomer 2.0-HT (020234 by Olympus America Inc.) with scanning mode of x20 (0.46 μm/pixel) either automatic or semi-automatic set up under SOP (MICR 1.1.03) at the department of Pathology and RHLCCC Core Facility of Northwestern University. The digital images were then stored as high definition and were analyzed with NDP (NanoZoomer Digital Pathology, Hamamatsu Inc.) View software (https://www.hamamatsu.com/us/en/product/type/U12388-01/index.html) for quantification analysis. For identification of individual nuclei in the tissue, we trained a Cell Classifier in the Visiopharm Image analysis Suite (VIS, Horsholm, Denmark) by manually annotating exemplar nuclei that were positive and negative for DAB (DAB+ and DAB-, respectively). Once the Cell Classifier was trained, we applied the trained Cell Classifier to all images to generate counts of DAB+ and DAB- nuclei and calculate a percent positive index. Three sets of tumors and two sets of spleens were analyzed for Ly6G, CD11b and TUNEL staining; in set 1 the entire tumor of multiple slides from 4T1 wt and CD95 k.o. in BALB/c mice were scanned, average percent positive cells for Ly6G and CD11 were determined. In set 2, either the entire tumor or 3 selected independent fields from pure tumor in multiple slides were quantified as average percent positive cells for TUNEL stain from 4T1 wt and CD95 k.o. in BALB/c mice treated with IgG or anti-CD8 Ab. Set 3 included the quantification of Ly6G staining in the entire tumor of multiple slides from 4T1 wt and CD95 k.o. tumors in NSG mice. Set 4 was the quantification of CD8, CD4, or NKp46 positive cells in spleens of depleted mice.

RNA-seq library construction from cell lLines grown *in vitro*

Total RNA from cells (U-clones) was extracted using TRIzol (Invitrogen 15596018). mRNAs were enriched using Oligo d(T)25 Magnetic Beads (NEB S1419S) following manufacturer's protocol. mRNAs were then fragmented at 94°C in 10 mM MgCl2 buffer. Fragmented RNAs were end-repaired by T4 PNK (NEB M0201S) and poly(A)-tailed by E. coli Poly(A) Polymerase (NEB M0276S). The poly(A) tailed RNA fragments were reverse transcribed to cDNA using custom-designed oligo(dT) and locked nucleic acid (LNA) based on SMART-seq2 method (Picelli et al., 2014). The cDNAs were then PCR amplified using KAPA HiFi HotStart master mix (KK2601). 200-400 bp fragments of the library were cut from gels for Illumina Hiseq sequencing.

RNA-seq library construction from tumors grown *in vivo*

For the RNA sequencing wt and CD95 k.o. 4T1 tumors were isolated from NGS and Balb/c mice and tumor tissues were store in RNA later solution until further use. For RNA isolation tumor tissue was lysed using Qiazol and total RNA was isolated using the miRNeasy Mini Kit (Qiagen, Cat.No# 74004) following the manufacturer's instructions. An on-column digestion step using the RNAse-free DNAse Set (Qiagen, Cat.No# 79254) was included for all RNA-Seq samples. RNA libraries were generated and sequenced (Genomics Core at Northwestern University). The quality of reads, in FASTQ format, was evaluated using FastQC. Reads were trimmed to remove Illumina adapters from the 3' ends using cutadapt (Martin, 2011). Trimmed reads were aligned to the mouse genome (m38/mm10) using STAR (Dobin et al., 2013). Read counts for each gene were calculated using htseq-count (Anders et al., 2015) in conjunction with a gene annotation file for m38 obtained from Ensembl (http://useast.ensembl.org/index.html). Normalization and differential expression were calculated using DESeq2 that employs the Wald test (Love et al., 2014). The cutoff for determining significantly differentially expressed genes was an FDR-adjusted p-value less than 0.05 using the Benjamini-Hochberg method.

RNA-seq and gene ontology data analysis

We used the first end of the sequencing reads for the analyses. The raw reads were filtered to remove low-quality reads using FASTQ Quality Filter from FASTX-Toolkit v0.0.14 (RRID:SCR_005534). High-quality reads were then mapped to the mouse reference genome (mm10) using STAR v2.6.0 (RRID:SCR_015899) with the following options to generate BAM files, count files, and read coverage tracks: –outSAMtype BAM SortedByCoordinate –quantMode TranscriptomeSAM GeneCounts –outWigType bedGraph –outWigNorm RPM. The transcriptomic BAM file was used to quantify gene expression using RSEM v1.3.0 (RRID:SCR_013027). Differential gene expression analysis was carried out on the gene counts using DESeq2 (RRID:SCR_015687). Gene expression (log2(TPM + 1)) was normalized to the mean of the corresponding control samples and significantly differentially expressed genes (DESeq2 adjusted p-value < 0.05) were clustered into 6 groups using k-means clustering. Gene ontology analysis was performed for each cluster using the TopGO package (RRID:SCR_014798). Heatmaps were created with the pheatmap package v1.0.12 (RRID:SCR_016418). All analyses were carried out using R v3.6.3 (RRID:SCR_001905). The GO enrichment analyses shown in Figure 3B was performed using the GOrilla gene ontology analysis tool at http://cbl-gorilla.cs.technion.ac.il using default settings and a p-value cut-off of 10^{-6}.

QUANTIFICATION AND STATISTICAL ANALYSIS

All experiments were performed in triplicate. The results were expressed as mean ± SD and analyzed by the Student's two-tailed t test or by two-way ANOVA (Prism8). Statistical significance was defined as $p < 0.05$.

ADDITIONAL RESOURCES

This study has not generated or contributed to a new website/forum and is not part of a clinical trial.